

*i*improved MASTER for the LSS: Fast and accurate analysis of the two point power spectra and correlation functions

Sukhdeep Singh^{1,2*}

¹*McWilliams Center for Cosmology, Department of Physics, Carnegie Mellon University, Pittsburgh, PA 15213, USA*

²*Berkeley Center for Cosmological Physics, University of California, Berkeley, CA 94720, USA*

Accepted XXX. Received YYY; in original form ZZZ

ABSTRACT

We review the methodology for measurements of two point functions of the cosmological observables, both power spectra and correlation functions. For pseudo- C_ℓ estimators, we will argue that the window weighted overdensity field can yield more optimal measurements as the window acts as an inverse noise weight, an effect that becomes more important for surveys with a variable selection function. We then discuss the impact of approximations made in the MASTER algorithm and suggest improvements, the *i*MASTER algorithm, that uses the theoretical model to give unbiased results for arbitrarily complex windows provided that the model satisfies weak accuracy conditions. The methodology of *i*MASTER algorithm is also generalized to the correlation functions to reconstruct the binned power spectra, for E/B mode separation, or to properly convolve the correlation functions to account for the scale cuts in the Fourier space model. We also show that the errors in the window estimation lead to both additive and multiplicative effects on the over density field. Accurate estimation of window power can be required up to scales of $\sim 2\ell_{\text{max}}$ or larger. Misestimation of the window power leads to biases in the measured power spectra which scale as $\delta C_\ell \sim M_{\ell\ell'}^W \delta W_{\ell'}$, where the $M_{\ell\ell'}^W$ scales as $\sim (2\ell + 1)C_\ell$ leading to effects that can be important at high ℓ . While the notation in this paper is geared towards photometric galaxy surveys, the discussion is equally applicable to spectroscopic galaxy, intensity mapping and CMB surveys.

Key words: cosmology: observations — large-scale structure of Universe — gravitational lensing: weak

1 INTRODUCTION

The measurements of the large scale structure (LSS) in the universe provide important cosmological information about the evolution of the universe over time and also allow us to study the physical properties of its constituents, namely Dark matter, Dark energy, neutrinos and baryons (see Weinberg et al. 2013, for a review). Over the past two decades we have successfully measured the LSS using a number of probes, e.g. baryon acoustic oscillations and galaxy velocities (e.g. Alam et al. 2016; Neveux et al. 2020), weak gravitational lensing (e.g. Planck Collaboration et al. 2020; DES Collaboration et al. 2017; Singh et al. 2020; Heymans et al. 2021), galaxy clusters (e.g. Abbott et al. 2020). These measurements have yielded strong constraints on the cosmological models with precision of order 5-10%. There are also some tensions among the probes at $2 - 3\sigma$ signifi-

cance level (DES Collaboration et al. 2017; Singh et al. 2020; Heymans et al. 2021; Di Valentino et al. 2020; Lange et al. 2021) that have been a source of general intrigue and excitement in the community and also require us to revisit many of the assumptions made in the analysis. With upcoming percent level measurements from the planned surveys, e.g. Rubin Observatory LSST-DESC (LSST Dark Energy Science Collaboration 2012), DESI (Levi et al. 2019), Roman space telescope (Dore et al. 2019), Simons Observatory (Ade et al. 2019), CMB-S4 (Abazajian et al. 2016), Sphex (Doré et al. 2014), it is going to become even more important for us to thoroughly understand the analysis in order to derive accurate inferences on cosmological models. In this paper we will review the methodology for the measurements of the two point statistics of the over density field from the LSS surveys.

The large scale structure measurements from the cosmological surveys are made by turning the data from the survey into the maps of over density field, which is the quan-

* E-mail: sukhdeep@cmu.edu

tity of interest in measuring the fluctuations in the matter density. Correlations of mean zero overdensity field have also been shown to be more optimal than the density field with non-zero mean (Landy & Szalay 1993; Singh et al. 2017). In this paper, by optimal we will usually mean minimizing some combination of bias and variance in the inferences. The maps of over density are then compressed using the summary statistics, especially the two point correlation functions or power spectra, which are a measure of the variance in the field. During the process of these measurements there are several questions that one needs to address to ensure the optimality of the measurement as well as the accuracy of the inferences derived from these measurements.

After the data is acquired and cleaned, the analysis begins with the process of map making (or making catalogs), whereby we bin the count of galaxies (or photons in case of intensity mapping) into pixels of a map. One of the questions that we need to address at this stage is the weighting to be applied to the pixels to ensure optimal analysis. The question of optimal weights for the case of gaussian random fields has been addressed by Feldman et al. (1994) giving us the famous FKP weights, which was later generalized by Hamilton (1997). While FKP weights (or quadratic estimator in general) has been shown to be optimal for the gaussian field, it is computationally expensive to use such weights in practice and instead the pseudo- C_ℓ like estimators (Wandelt et al. 2001) are preferred. In such estimators, it is fairly common to adopt uniform weighting, which is usually not optimal.

The next step in the analysis is to measure the power spectra or the correlation functions of the over density field. In this step, one of the major challenges is to account for the effects of the survey window. The survey window or the selection function depends on the survey geometry (mask) as well as the any observational selection effects and the weights applied on the maps as discussed earlier. The modeling of window effects on the pseudo- C_ℓ power spectra has been addressed in detail by Hivon et al. (2002) who introduced the now standard MASTER algorithm to deconvolve the effects of the window to reconstruct the power spectra of the underlying fields. Similarly, formalism for the measurement of the correlation functions was developed by Ng & Liu (1999). The window also affects the correlation functions in a very similar manner by acting as a weighting function and changing the effective scale of measurement (see e.g. appendix D of Singh et al. 2020).

Since proper modeling of the two point functions requires careful modeling of the window effects, one of the major challenges in the LSS measurements is to properly estimate the window. Biases in the window estimation directly propagate into both the power spectra and the correlation functions. The strategies to model window biases include the mode deprojection (Slosar et al. 2004; Leistedt et al. 2013; Elsner et al. 2017) where one can subtract out systematics or down weight the affected modes by including additional terms in the covariance. Similar strategies have also been applied for the case of the correlation functions, e.g. Ross et al. (2012).

The final step before running the inference is to implement the ‘scale cuts’ on the measurements to match the scales of the model. Typically the models we use to analyze the data are validated under certain assumptions and can

only model a limited range of scales which is smaller than the range of scales probed by the current data. Applying these scale cuts carefully is necessary for the optimal analysis, i.e. to extract as much information as possible while avoiding the biases from the model outside its range of validity. Recently this issue of scale cuts has shown up in some apparent discrepancies between the analysis in the configuration space (correlation functions) and the Fourier space (power spectra) (see Hamana et al. 2020; Doux et al. 2021). Such issues are concerning as they complicate the interpretation of the inferences drawn from the analysis and need to be carefully addressed.

In this paper we will review the methodology described above, study the optimality of the weights applied on the over density field during the pseudo- C_ℓ like analysis and also test the assumptions made in the methods to model the window functions. Since modeling the window function is important and also very challenging, we will study the impact of the window mis-estimation on the two point functions (we will not discuss the methods to estimate the window, only the methods to account for window mis-estimation). Finally, we will generalize the MASTER algorithm to the correlation functions to study the impact of the scale cuts and devise new methods for more optimal scale cuts. We will use the notation commonly used in the analysis of the angular statistics. However, most of our discussion will be equally applicable to the analysis of the spectroscopic surveys, both galaxies and intensity mapping ones.

The simulations and power spectra calculations for window modeling are performed using the HEALPY (Górski et al. 2005) package, the matter power spectra is obtained using CAMB¹ package and the computations of angular power spectra, coupling matrices, correlation functions and any other relevant calculations are performed using the SKYLENS package (Singh et al. in prep).

2 MAP MAKING

We begin with a brief the discussion of turning the catalogs of observables from the telescopes to the maps of the over density fields. For the case of galaxy counts (or intensity mapping), the observed number of galaxies at a position \mathbf{x} can be described as

$$n_g(\mathbf{x}) = \langle n_g(\mathbf{x}) \rangle (1 + \delta_g(\mathbf{x})), \quad (1)$$

where $\langle n_g(\mathbf{x}) \rangle$ is the ensemble average of $n_g(\mathbf{x})$ and can be thought of as the expected number of galaxies to be observed at position \mathbf{x} ignoring the effects of noise and the over density field. $\delta_g(\mathbf{x})$ is the overdensity of galaxies at \mathbf{x} . We will also use the mean of $\bar{n}_g(\mathbf{x})$ over the whole survey,

$$\bar{n}_g = \bar{n}_g(\mathbf{x}). \quad (2)$$

Throughout this paper, $\langle \rangle$ implies the ensemble average of the quantity inside the brackets, which implies an average over many realizations of data and \bar{X} represents the sample mean of quantity X , where by sample mean we will usually imply mean over the given realization of the survey. Quantities with tophat, e.g. $\hat{\delta}$, represent the measurements from data.

¹ <http://camb.info>

From eq. (1), a simple way to define windowed over density field is

$$\hat{\delta}_{g,W}(\mathbf{x}) = \frac{\langle n_g(\mathbf{x}) \rangle}{\bar{n}_g} (1 + \delta_g(\mathbf{x})) - \frac{\langle n_g(\mathbf{x}) \rangle}{\bar{n}_g} = W_g(\mathbf{x}) \delta_g(\mathbf{x}), \quad (3)$$

In the second equality, we defined the window function (or selection function) as

$$W_g(\mathbf{x}) = \frac{\langle n_g(\mathbf{x}) \rangle}{\bar{n}_g} = 1 + F(C_i(\mathbf{x})). \quad (4)$$

$W_g(\mathbf{x})$ is the selection function which accounts for the observational effects in the survey which modulate the observed density of the galaxies. In the second part of the equation we wrote the window as function of underlying contaminants, C_i . In general F can be a non-linear function and a detailed discussion of window estimation is outside the scope of this work (see Ross et al. 2020; Rezaie et al. 2020; Everett et al. 2020, for some recent work). We will only focus on the effects of the window on statistics of interest, namely the two point correlations of the fields. We will discuss the effects of window miss-estimation in section 2.2 and in later sections on how it propagates into the two point correlations of the fields. In this work it is also assumed that the window function and the underlying over-density field are uncorrelated. This is in general not true as the window function is correlated with the underlying field due to observational effects such as blending and fiber collisions. Detailed discussion of such effects is left for the future work.

A more popular choice for defining over density maps is to remove the effects of window by dividing with $\langle n_g(\mathbf{x}) \rangle$ (or $W_g(\mathbf{x})$ as discussed above), in which case we get

$$\hat{\delta}_g(\mathbf{x}) = \frac{n_g(\mathbf{x})}{\langle n_g(\mathbf{x}) \rangle} - 1 = \frac{n_g(\mathbf{x})}{W_g(\mathbf{x}) \bar{n}_g} - 1 = \delta_g(\mathbf{x}), \quad (5)$$

which is free from the effects of window. This is not strictly true as the mask effects are still present and typically mask also needs to be modified to remove the pixels where $W_g(\mathbf{x})$ is small.

Many studies in the literature work with the galaxy catalogs instead of maps (see also discussion in section 4.1). In such a case, if we apply systematics weights on galaxies to correct for window effects and use uniform randoms, i.e. $\langle n_R(\mathbf{x}) \rangle / \bar{n}_g = 1$, where n_R is the number of randoms, we get the estimator in eq. (5) (e.g. Ross et al. 2012; Alam et al. 2016; Elvin-Poole et al. 2018), i.e.,

$$\hat{\delta}_g(\mathbf{x}) = \frac{n_g(\mathbf{x})/W_g(\mathbf{x}) - n_R(\mathbf{x})}{n_R(\mathbf{x})} = \frac{n_g(\mathbf{x})}{W_g(\mathbf{x}) \bar{n}_g} - 1. \quad (6)$$

On the other hand, if the systematics weights are applied on the randoms, i.e. $\langle n_R(\mathbf{x}) \rangle / \bar{n}_g = W_g(\mathbf{x})$, then we obtain the estimator from eq. (3), i.e.,

$$\hat{\delta}_{g,W}(\mathbf{x}) = \frac{n_g(\mathbf{x}) - n_R(\mathbf{x})}{\bar{n}_g} \quad (7)$$

In eq. (3), Window (W_g) acts as weight on the pixels in the map and turns out to be a nearly optimal way to apply the weights. In general, optimal weights for the power spectra estimation of a gaussian random field are (Feldman et al. 1994; Hamilton 1997)

$$W_{FKP}(\mathbf{x}) \propto (C_\ell + N_\ell(\mathbf{x}))^{-1}, \quad (8)$$

where C_ℓ is the power spectra of the mode of interest and $N_\ell(\mathbf{x}) = 1/n_g(\mathbf{x})$ is the noise power spectra. This is the inverse variance weighting where C_ℓ accounts for the sample (cosmic) variance and N_ℓ accounts for variance contributed by the noise. Note that the FKP weights are sometimes written as, $w \propto 1/(1 + n(\mathbf{x})C_\ell)$. This definition of weights is valid when the weights are applied to galaxies, while the weights we define in eq. (8) are applied to the pixels of the over density maps.

In the noise dominated regime, ($N_\ell \gg C_\ell$), the FKP weights reduce to W_g in eq. (4). In general the FKP weights depend on the power spectra mode being measured and for a tomographic survey with multiple redshift and ℓ bins, the proper use of FKP weight for optimal analysis can be computationally expensive. Hence pseudo- C_ℓ estimators with a single weighting scheme are usually preferred in practice. For such a case, FKP like weights can be defined by fixing $C_\ell = C_0$, where C_0 is power spectra at some fixed chosen ℓ . The overdensity field from eq. (3) is then modified to

$$\hat{\delta}_{g,FKP_0}(\mathbf{x}) = \frac{\langle n_g(\mathbf{x}) \rangle}{\bar{n}_g} \frac{1 + \bar{n}_g C_0}{1 + \langle n_g(\mathbf{x}) \rangle C_0} \delta_g(\mathbf{x}), \quad (9)$$

These weights are similar to those in eq. (4), except that C_0 here modulates the weights at the higher end to prevent few pixels from having very large weights which can increase the cosmic variance.

The maps for other observables such as galaxy shear can be defined analogously to eq. (3) as

$$\hat{\gamma}_{i,j}(\mathbf{x}) = \frac{n_g(\mathbf{x})}{\bar{n}_g} \gamma_{i,j}(\mathbf{x}) = W_\gamma(\mathbf{x}) \gamma_{i,j}(\mathbf{x}), \quad (10)$$

where the window $W_\gamma(\mathbf{x})$ depends on the observed number of galaxies in the pixel (as opposed the expected number of galaxies in W_g)

$$W_\gamma(\mathbf{x}) = \frac{n_g(\mathbf{x})}{\bar{n}_g} = 1 + F(C_i(\mathbf{x})) + \delta_g(\mathbf{x}). \quad (11)$$

$W_\gamma(\mathbf{x})$ is relatively easier to estimate compared to W_g since it is determined by the position of the source galaxies. That being said, the effects of varying photometry on the shear estimation can be thought of as part of the window and hence the problems associated with the window estimation we discuss later in this paper are applicable to galaxy shear estimation as well. The FKP like weights can also be defined for shear noting that shape noise scales as $\sigma_e^2/n_g(\mathbf{x})$, resulting in

$$\hat{\gamma}_{i,j,FKP}(\mathbf{x}) = \frac{n_g(\mathbf{x})}{\bar{n}_g} \frac{\sigma_e^2 + \bar{n}_g C_0}{\sigma_e^2 + n_g(\mathbf{x}) C_0} \gamma_{i,j}(\mathbf{x}). \quad (12)$$

For the case of intensity mapping surveys, the window, $W(\mathbf{x})$, is same as the mean intensity term, \bar{I} (up to a constant), that is sometimes used (e.g. Schaan & White 2021). In fact $W(\mathbf{x})$ is a generalization of the \bar{I} term in Schaan & White (2021) as we allow for the effects such as foregrounds, detector calibration, etc. to vary over the positions \mathbf{x} . While Schaan & White (2021) suggested that cross correlations may be useful in determining \bar{I} under certain assumptions, unfortunately the cross correlations in a general case may not be of much help with the window modeling. This is because different tracers/surveys have (at least partially) uncorrelated windows and hence the sensitivity of cross correlations to the window is very different from the sensitivity

of the auto correlations. We will see an example of such an effect in section 3.

In this work, we will restrict ourselves to the pseudo- C_ℓ like analysis and will use the weighting scheme of eq. (4) and (10), which is more optimal in most cases than no weighting in (5) (see also discussion in section 2.1). It should be remembered that this weighting scheme increases the cosmic variance and in many practical applications weighting of eq. (9) and (12) can be more optimal.

2.1 Shot noise

Under the assumption that the sampling of the discrete tracers follow Poisson distribution, the noise in observed number of galaxies in each pixel is given by

$$\langle n_g^2(\mathbf{x}) \rangle = \langle n_g(\mathbf{x}) \rangle. \quad (13)$$

When the galaxies are assigned weights, w , the noise changes to (Bohm & Zech 2014, we assume weights are deterministic)

$$\langle n_{g,w}^2(\mathbf{x}) \rangle = \langle n_g(\mathbf{x}) \rangle w(\mathbf{x})^2. \quad (14)$$

The over density field of eq. (3) assigns weights of $1/\bar{n}_g$ to each galaxy, in which case the noise is given by

$$\langle \delta_{N,W}^2(\mathbf{x}) \rangle = \frac{\langle n_g(\mathbf{x}) \rangle}{\bar{n}_g^2} = W_g(\mathbf{x}) \frac{1}{\bar{n}_g}. \quad (15)$$

Averaging over the whole survey, we get

$$\langle \overline{\delta_{N,W}^2} \rangle = \overline{W_g(\mathbf{x})} \frac{1}{\bar{n}_g}. \quad (16)$$

Notice that in eq. (15), two powers of noise, δ_N^2 , depend on a single power of W_g . Therefore the noise is effectively multiplied by the window given by $\sqrt{W_g(\mathbf{x})}$ (Feldman et al. 1994; Li et al. 2019), i.e.,

$$\sqrt{\langle \delta_{N,W}^2 \rangle}(\mathbf{x}) = \sqrt{W_g(\mathbf{x})} \frac{1}{\sqrt{\bar{n}_g}}. \quad (17)$$

Similarly for the over density field in eq. (5), noise is given by

$$\langle \delta_N^2 \rangle(\mathbf{x}) = \frac{1}{\langle n_g(\mathbf{x}) \rangle} = \frac{1}{W_g(\mathbf{x}) \bar{n}_g}. \quad (18)$$

Averaging over the whole survey, we get

$$\langle \overline{\delta_N^2} \rangle = \left[\frac{1}{\overline{W_g(\mathbf{x})}} \right] \frac{1}{\bar{n}_g}. \quad (19)$$

With $\overline{W_g(\mathbf{x})} = 1$ and $W_g(\mathbf{x}) \in [0, \infty)$ by construction, it can be shown via Jensen's inequality that (see also appendix A for an alternate proof)

$$\left[\frac{1}{\overline{W_g(\mathbf{x})}} \right] \geq \overline{W_g(\mathbf{x})}. \quad (20)$$

Thus the estimator in eq. (3) is in general has lower noise than the estimator of eq. (5). Both estimator give very similar signal when $\overline{W_g(\mathbf{x})} = 1$. Qualitatively, this is because the power spectra measurement, pseudo- C_ℓ , depends on the window power spectra which is the second power of window while the noise depends on the first power of window. Hence the choice of estimator has stronger effect on noise than on signal. We will also compute the response of the pseudo- C_ℓ power spectra estimator to the window power spectra in

section 3.4 and show that the response is positive, implying that the estimator in eq. (3) will give larger signal in pseudo- C_ℓ since it will in general have higher window power. This further increases the signal to noise ratio of the estimator in eq. (3) with respect to the estimator in eq. (5).

The inequality in eq. (20) will get worse as the window becomes more complex ($W_g(\mathbf{x})$ distribution get wider). Some times arguments are made in favor of using eq. (5) to simplify the window modeling but instead it becomes more important to use eq. (3) (or eq. (9)) for more complex windows.

A corollary to eq. (20) is that with the estimator of eq. (5), using $1/\bar{n}_g$ to model the noise effects in the covariance (analytical or mocks with overly simplified window) will lead to under estimation of the such effects during the analysis, unless the window effects are properly modeled. One simple method is to modify the effective number density of galaxies, but it can still leads to biases in the cross covariance terms of the form $N_\ell C_\ell$, where N_ℓ is the noise power spectra.

Also, we only considered the galaxy shot noise as source of variance in this section. In appendix B, we derive similar expression in presence of additional source of noise as well as weighting applied to galaxies. For the main part of this paper, we will continue using the galaxy shot noise only version of equations to keep the notation and discussion simpler. The results of the paper do not change for the case considered in appendix B.

While in this paper we only consider noise correlated at zero lag, it is worth remembering that in the general case correlated noise will also depend upon the window and the window for noise is different from the window for the underlying over density field. Thus window effects on noise need to be modeled separately, both for mean noise subtraction from the power spectra measurement as well as in the covariance of both power spectra and correlation functions. The code, SKYLENS, used in this paper is able to handle noise with any user input power spectra and window function.

2.2 Window bias

In eq (4), we defined window as a function of some underlying contaminants. Even if those contaminants are known, we still need to estimate the response of the selection function to these contaminants in order to estimate the window. This is a non-trivial task and usually there will be some errors in estimating these responses, in which case our estimates of window can be biased. Without the loss of generality, we can write the estimated window as

$$\widehat{W}_g(\mathbf{x}) = (1 + m(\mathbf{x})) W_g(\mathbf{x}), \quad (21)$$

where $W_g(\mathbf{x})$ is the true underlying window and $m(\mathbf{x})$ denotes the relative error in the estimated window.

With the erroneous window defined in eq. (21), our estimate of the over-density fields become

$$\widehat{\delta}_{g,W,m}(\mathbf{x}) = \frac{n_g(\mathbf{x})}{\bar{n}_g} - \frac{\langle \widehat{n_g(\mathbf{x})} \rangle}{\bar{n}_g}, \quad (22)$$

where $\langle \widehat{n_g(\mathbf{x})} \rangle$ is the biased estimate of the expected number of galaxies. Writing the observed number of galaxies, $n_g(\mathbf{x})$ in terms of the true window and the over density field, we

get

$$\begin{aligned}\hat{\delta}_{g,W,m}(\mathbf{x}) &= W_g(\mathbf{x})\delta_g(\mathbf{x}) - \delta W_g(\mathbf{x}) \\ &= \frac{\widehat{W}_g(\mathbf{x})}{1+m(\mathbf{x})}\delta_g(\mathbf{x}) - \delta W_g(\mathbf{x}).\end{aligned}\quad (23)$$

Where in the second step we wrote the true window in terms of the biased estimate, since that is the window we use in modeling. When m is small, the multiplicative bias can be estimated as $\sim -\widehat{W}_g(\mathbf{x})m(\mathbf{x})$.

For the over density field defined in eq. (5), we can write the effects of bias as

$$\hat{\delta}_{g,m}(\mathbf{x}) = \frac{\delta_g(\mathbf{x}) - m(\mathbf{x})}{1+m(\mathbf{x})}. \quad (24)$$

Both estimators, $\hat{\delta}_{g,W,m}$ and $\hat{\delta}_g$ contain the multiplicative bias of $O(m\delta)$ and an additive bias of $O(m)$.

If mW_g is a bias (as opposed to random noise) and is small, we can assume the bias in the window is a linear combination of the underlying contaminants (e.g. Leistedt et al. 2013), C_i ,

$$\delta W_g(\mathbf{x}) = m(\mathbf{x})W_g(\mathbf{x}) \approx \sum \alpha_i C_i(\mathbf{x}). \quad (25)$$

Where α_i are the unknown amplitudes. It is important to stress here that we are only ‘assuming’ the biases in the window function as linear function of contaminants and we do not assume the window function itself to be a linear function of the underlying contaminants. The additive biases can sometimes be constrained by cross-correlating the over density maps with the maps of systematics (Ross et al. 2012; Leistedt et al. 2013). We will study the effects of multiplicative bias in the section 3.4.

Finally it is worth mentioning that the multiplicative and additive biases in the shear estimation can also be thought of as part of the window in a similar vein as above and our discussion of the window systematics here and in later sections is applicable to all tracers.

3 POWER SPECTRA

Once the over density maps are generated, the next step in the standard two point analysis is to compute the power spectra or the correlation functions of the maps. In this section we will discuss the power spectra of the windowed maps, the algorithm to model the window effects and the methods to account for the uncertainties in the window estimation.

3.1 Pseudo- C_ℓ power spectra

Since the observed over density field is multiplied by the window, its Fourier transform² is convolved with the Fourier transform of the window. Computing the power spectra of this windowed field results in the pseudo- C_ℓ estimator (D_ℓ), whose expected value is related to the true power spectra via a coupling matrix (Hivon et al. 2002),

$$\hat{D}_\ell = M_{\ell\ell'} C_{\ell'} + M_{\ell\ell'}^N N_{\ell'}, \quad (26)$$

² We will use Fourier transform to describe both flat sky Fourier transform and the spherical harmonics transform in curved sky

where $M_{\ell\ell'}$ is the coupling matrix for the signal part and $M_{\ell\ell'}^N$ is the coupling matrix for the noise in the observed field (as discussed in section 2.1 noise and signal have a different window). Here summation over ℓ' is implied and throughout the paper we will use the Einstein summation convention to imply sum over repeated indices. To keep notation simpler, we will omit the noise term from the equations. This will not affect our discussion since it is easy to generalize to the noise case.

The coupling matrices is given by

$$\begin{aligned}M_{\ell,\ell'} &= \frac{(2\ell'+1)}{4\pi} \sum_{\ell''} W_{\ell''}(2\ell''+1) \begin{pmatrix} \ell & \ell' & \ell'' \\ s_1 & -s_1 & 0 \end{pmatrix} \\ &\quad \times \begin{pmatrix} \ell & \ell' & \ell'' \\ s_2 & -s_2 & 0 \end{pmatrix},\end{aligned}\quad (27)$$

where ℓ, ℓ' are as defined in eq. (26), $W_{\ell''}$ is the power spectra (pseudo- C_ℓ) of the window defined at ℓ'' (cross power spectra of two windows for cross correlations), s_1, s_2 are the spins of the two tracers being correlated to obtain the \hat{D}_ℓ .

For the case of spin-2 quantities, e.g. galaxy shear or CMB polarization, the power spectra of E and B modes is given by,

$$D_\ell^{EE} = M^+ C_\ell^{EE} + M^- C_\ell^{BB} \quad (28)$$

$$D_\ell^{BB} = M^+ C_\ell^{BB} + M^- C_\ell^{EE}. \quad (29)$$

In the second equality we wrote E/B pseudo-power spectra in terms of true E/B power spectra using spin-2 coupling matrices, given by

$$\begin{aligned}M_{\ell,\ell'}^\pm &= \frac{(2\ell'+1)}{4\pi} \sum_{\ell''} W_{\ell''}(2\ell''+1) \left(\frac{1 \pm (-1)^{\ell+\ell'+\ell''}}{2} \right) \\ &\quad \times \begin{pmatrix} \ell & \ell' & \ell'' \\ 2 & -2 & 0 \end{pmatrix} \begin{pmatrix} \ell & \ell' & \ell'' \\ 2 & -2 & 0 \end{pmatrix}.\end{aligned}\quad (30)$$

In this section we will assume that the B -mode power spectra is zero, i.e. $C_\ell^{BB} = 0$ and will therefore only use $D_\ell^{EE} = M^+ C_\ell^{EE}$ and $D_\ell^{BB} = M^- C_\ell^{EE}$. We will discuss the more general case in section 4.2.1. Hereafter, we will also drop the superscripts \pm, EE, BB on the M and power spectra unless necessary for clarity.

In general $M_{\ell,\ell'}$ is a rectangular matrix with $\ell'_{\max}, \ell''_{\max} \gg \ell_{\max}$. In practice, the modern survey windows are large enough (narrow in Fourier space) such that with $\ell_{\max} \sim O(1000 - 5000)$ and $C_\ell \propto \ell^{-2}$, $\ell'_{\max} \sim \ell_{\max}$ approximation is sufficient for accuracy of up to few percent near ℓ_{\max} (the examples shown later in this section satisfy this assumption). With such an approximation, we need to estimate the window up to $\ell'' \sim 2\ell_{\max}$. These approximation however may not work if the window has large enough power out to very high ℓ'' or in the case when the power spectra does not fall fast enough with ℓ (e.g. noise spectrum). In such a case $\ell'_{\max} \gg \ell_{\max}$ maybe necessary or one may have to resort to trickery such as apodizing the window in order to tame the coupling matrix. We will discuss an example of such effects in a later section when we reconstruct power spectra from correlation functions.

3.2 MASTER algorithm

As discussed in the previous section, one of the challenges in the pseudo- C_ℓ analysis is that $M_{\ell\ell'}$ is an $O(\ell_{\max}^2)$ matrix

where $\ell_{\max} \sim 1000 - 5000$ or even larger. While computation of $M_{\ell\ell'}$ can be easily handled on the modern day computers, it is still desirable to reduce the dimensionality of the $M_{\ell\ell'}$ for the purpose of sampling during the inference. De-convolving unbinned D_ℓ to reconstruct C_ℓ by inverting eq. (26) is also not straight forward in the presence of large noise (remember noise has a different coupling matrix and noise contributions scale as $M^{-1}[M^N(N_\ell) - \langle M^N(N_\ell) \rangle]$). Thus it is generally desirable to bin the noisy D_ℓ measurements to reduce noise effects. Hivon et al. (2002) presented the MASTER algorithm which allows us to work with binned quantities, reducing the complexity of the problem to $O(N_b^2)$, where N_b is the number of bins.

In the MASTER algorithm, we simply write the eq. (26) in terms of the binned quantities,

$$\hat{D}_{\ell_b} = M_{\ell_b, \ell'_b} C_{\ell'_b} + N_{\ell'_b}. \quad (31)$$

The binned M_{ℓ_b, ℓ'_b} is given by

$$M_{\ell_b, \ell'_b} = P_{\ell_b, \ell} M_{\ell\ell'} Q_{\ell', \ell'_b}, \quad (32)$$

where $P_{\ell_b, \ell}$ and Q_{ℓ', ℓ'_b} are binning and inverse binning operations respectively and can be analytically written under the assumption that $\ell(\ell+1)C_\ell \sim \text{constant}$,

$$P_{\ell_b, \ell} = \begin{cases} \frac{1}{2\pi} \frac{\ell(\ell+1)}{\Delta\ell_b}, & \ell \in b \\ 0 & \text{otherwise} \end{cases}, \quad (33)$$

$$Q_{\ell, \ell_b} = \begin{cases} \frac{2\pi}{\ell(\ell+1)}, & \ell \in b \\ 0 & \text{otherwise} \end{cases}, \quad (34)$$

where $\ell \in b$ is true when ℓ belongs to the bin centered on ℓ_b and $\Delta\ell_b$ is the bin size. In some implementations of the MASTER algorithm, C_ℓ is assumed to be constant within the bin (e.g. Alonso et al. 2019), in which case P and Q take values of 0 or 1. We will refer to such approximation as cMASTER.

The eq. (31) can be inverted to reconstruct the power spectra from the pseudo- C_ℓ

$$\hat{C}_{\ell_b} = M_{\ell_b, \ell'_b}^{-1} D_{\ell'_b}, \quad (35)$$

where we have taken the pseudo-inverse of the binned coupling matrix.

In fig. 1, we see the comparison of the D_ℓ predictions using both MASTER and cMASTER algorithms. In fig. 1 as well as in most other demonstrations later in the paper, we will employ two choices of the window, W_1 and W_2 . W_1 is chosen to be a more realistic and is similar to the galaxy shear window where the sampling is determined by galaxy positions and hence window power spectra is similar to galaxy power spectra. For W_2 , we increase the complexity of window further by raising the power spectra of window further at some scales (see appendix F for further details). W_2 acts as a stress tests for our methodology and comparison with W_1 also allows us to see where and how the biases are introduced by different methods.

In fig. 1 we observe that as the complexity of the window increases, both algorithms result in biased predictions. This is because coupling matrix becomes broader with more complex window and since D_{ℓ_b} is effectively a weighted sum of C_ℓ , a broader coupling matrix increases the impact of biases introduced by the approximations made in the definition of binning operators P and Q . Furthermore, cMASTER

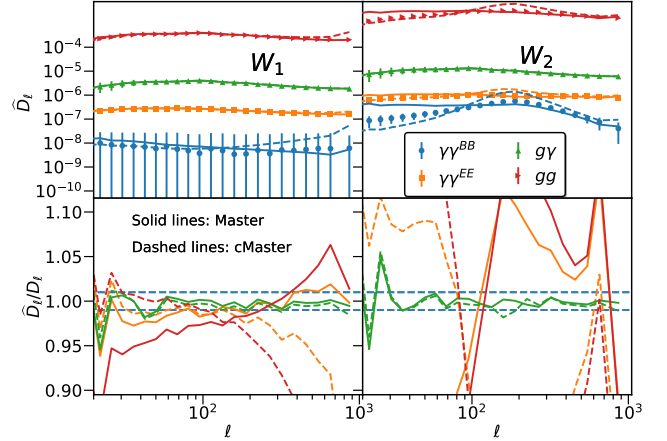


Figure 1. Comparison of binned pseudo- C_ℓ power spectra, D_ℓ , obtained from 1000 gaussian simulations (solid points with errorbars) and predictions obtained using MASTER (Hivon et al. 2002) and cMASTER (e.g. Alonso et al. 2019) algorithms, for auto and cross correlations between shear and galaxies. Left and Right panels show result from two different window functions, where W_1 is similar to the expected galaxy shear window while W_2 is more complex. Lower panel on each side shows the ratio between the simulations and the predictions, with horizontal dashed lines marking $\pm 1\%$ bias regions. Both MASTER and cMASTER in general give biased results and the magnitude of the bias increases with the complexity of the window.

has larger biases since it makes worse approximations in P and Q . These biases also propagate to the deconvolved power spectra (see fig. 2) and necessitate that some corrections be applied to the theory power spectrum before it can be compared with the biased estimators of either D_ℓ or deconvolved power spectra (see discussion in Alonso et al. 2019), i.e. we define:

$$C_{\text{cMaster}, \ell_b} = M_{\text{cMaster}, \ell_b, \ell'_b}^{-1} B_D M_{\ell' \ell''} C_{\ell''} = \mathcal{M}_{\text{cMaster}, \ell_b, \ell''} C_{\ell''}. \quad (36)$$

B_D is the binning operator similar to P and is defined in next section. In the second equality we defined $\mathcal{M}_{\text{cMaster}, \ell_b, \ell''} = M_{\text{cMaster}, \ell_b, \ell'_b}^{-1} B_D M_{\ell' \ell''}$. Using such an estimator is not strictly necessary, as one can simply work with the binned pseudo power spectra instead, i.e.

$$D_{\ell_b} = M_{\ell_b, \ell'} C_{\ell'}, \quad (37)$$

where $M_{\ell_b, \ell'} = B_D M_{\ell \ell'}$. This is a simple convolution+binning operation and will not be branded as MASTER algorithm in this paper.

In the next section we discuss the proper expression for P and Q which lead to recovery of unbiased results which can be compared directly with theory power spectra.

3.3 iMASTER

As discussed in the previous section, the biases in the MASTER algorithm are sourced by the assumptions made in implementing the effects of binning. Now we derive the MASTER algorithm without making such assumptions.

The binned version of eq. (26) can be written as

$$B_{D,\ell_b,\ell} D_\ell = B_{D,\ell_b,\ell} M_{\ell\ell'} B_{C,\ell',\ell_b}^{-1} B_{C,\ell',\ell} C_{\ell'} + B_{D,\ell_b,\ell} M_{\ell\ell'}^N B_{N,\ell',\ell_b}^{-1} B_{N,\ell',\ell} N_{\ell'}, \quad (38)$$

where B is the binning operator. We introduced separate binning operators, B_C , B_D and B_N , which operate on C_ℓ , D_ℓ , N_ℓ since the coupling matrix is not symmetric in general and ℓ , ℓ' can have different range. For examples shown throughout this work we will make the approximation that $\ell_{\max} \sim \ell'_{\max}$, (coupling matrix is not too wide) in which case $B_D = B_C$ can be used. We will simply assume $B_D = B_C = B$ and omit the subscripts hereafter unless required for clarity. Furthermore we assume noise is estimated and subtracted before binning and will neglect the effects of B_N as well. We will not assume any particular form for the binning operator and will keep our discussion general so that our method does not depend on the binning operator unlike the standard MASTER algorithm. We will discuss some particular forms of binning operator later in this section and the form of the binning operator used in examples of this paper is defined in eq. (45).

Binning data in general leads to loss of information and hence the binning operation can not be inverted. Thus B^{-1} in general is not defined. However, if we have good model for the underlying signal, then it is possible to obtain B^{-1} . In Hivon et al. (2002), model for C_ℓ was assumed to be $\ell(\ell+1)C_\ell \sim \text{constant}$ which allowed for an analytical expression for Q_{ℓ,ℓ_b} which is the inverse of binning operator $P_{\ell_b,\ell}$. However, since we hopefully have a better model for power spectra, the assumptions about C_ℓ are not necessary and we can simply write the inverse of binning operator as

$$B_{C,\ell,\ell_b}^{-1} = \begin{cases} \frac{C_\ell}{C_{\ell_b}}, \ell \in b \\ 0 \text{ otherwise} \end{cases}, \quad (39)$$

where $C_{\ell_b} = B C_\ell$ is obtained after binning the model C_ℓ and can be described as power spectra at some effective center of the bin, ℓ_b . The proper choice of ℓ_b is the effective ℓ at which the binned C_ℓ is measured and is given by

$$\ell_b = \frac{B_{C,\ell_b,\ell} C_\ell}{B_{C,\ell_b,\ell} C_\ell}. \quad (40)$$

The iMASTER binned coupling matrix is then

$$M_{\ell_b,\ell_b} = B_{D,\ell_b,\ell} M_{\ell\ell'} B_{C,\ell',\ell_b}^{-1}. \quad (41)$$

Fig. 2a shows the comparison of D_ℓ obtained using the iMASTER algorithm with that of 1000 gaussian simulations, similar to fig. 1. The model predictions are consistent with those of simulations to well within 1%, even for the case of more complex window W_2 . Figs. 2b-2d show the comparison of the C_ℓ reconstructed from the D_ℓ of simulations by convolving with the (pseudo) inverse of binned coupling matrix as described in eq. (35). Here again we observe that the iMASTER yield unbiased results to within 1% while both MASTER and cMASTER yield biased results as in the case of D_ℓ predictions in fig. 1.

It is important to stress here that the C_ℓ from the iMASTER algorithm can be directly compared with the un-binned theory computed at ℓ_b , i.e. the binning is performed analytically. This algorithm also does not require any additional correction to be applied unlike the method in eq. (36)

(Alonso et al. 2019). Furthermore, since the algorithm allows for cleaner reconstruction of C_ℓ , it is also more optimal in the analysis with scale cuts as it prevents the mixing of information between different scales in a much cleaner way. For example, in eq. (38) if we have scale cuts of form of $\ell' < \ell'_{\max}$, iMASTER prevents the information from $\ell' > \ell'_{\max}$ modes leaking into our analysis. At the same time the algorithm also captures the information about $\ell' < \ell'_{\max}$ modes which had leaked into high ℓ modes ($\ell > \ell'_{\max}$) of the pseudo- C_ℓ estimator (this requires $\ell_{\max} > \ell'_{\max}$ in eq. (38) and also using different binning operators B_D and B_C). These are the primary advantages of the iMASTER algorithm.

Due to B^{-1} , the estimator is now dependent on the underlying theoretical model. If one feels uncomfortable with such dependence, a half binned version, $M_{\ell_b,\ell'} = B_D M_{\ell\ell'}$ (see eq. (37)) can be used, with larger computational costs (both time and system memory). As discussed earlier, iMASTER is also more optimal in terms of scale cuts and preventing mixing of information between different scales. It may be advantageous to use iMASTER in the form similar to eq. (36), i.e.,

$$C_{i\text{MASTER},\ell_b} = M_{i\text{MASTER},\ell_b,\ell_b}^{-1} B_D M_{\ell'\ell''} C_{\ell''} = \mathcal{M}_{i\text{MASTER},\ell_b,\ell''} C_{\ell''}. \quad (42)$$

where $\mathcal{M}_{i\text{MASTER}}$ is computed at fiducial cosmology and is kept fixed. To reiterate, one of the advantages of iMASTER is that $C_{i\text{MASTER},\ell_b} = C_{\ell_b}$ and we can use the un-binned theory to compare with the measurements. Only in the case where the model varies strongly enough such that variations in iMASTER are significant compared to noise (while such variations are found to be small in our examples, similar tests should be performed at the time of analysis), using the form of eq. (42) will be necessary, where theory is properly binned using a fixed $\mathcal{M}_{i\text{MASTER}}$ computed with fiducial model. It should also be noted that the model dependence of iMASTER is weak, as B^{-1} is only sensitive to the slope of the power spectra within the bin. As long as the ratio does not vary significantly the model dependence should not introduce any significant biases. In fig. 2, the χ^2 per bin for different curves obtained using iMASTER is always less than 2/25 and for noiseless simulations (not shown) is less than 0.5/25. Therefore the model dependence introduced by iMASTER is not much different from the model dependence from other components in the analysis, e.g. converting distances to redshifts or computing covariance matrices at fixed cosmology. If the model dependence of iMASTER does matter in the inference problem, i.e. the bias due to assumptions in B^{-1} is larger than the uncertainties, it is also likely to be an indicative of a problem with binning, namely that bins are too wide and it maybe better to move to narrower bins to capture more information. It is not optimal to use overly broad bins with iMASTER. If using narrow bins is not possible, then obtaining model using eq. (42) may be necessary.

Now we discuss some particular forms of the binning operators. It should be remembered that in deriving the iMASTER algorithm we did not assume any particular form of the binning operators and any sensible choice of binning will work.

For noisy measurements with a given covariance, the binning operator can be defined using the optimal estimator of the mean D_ℓ within the bin (assuming gaussian distribu-

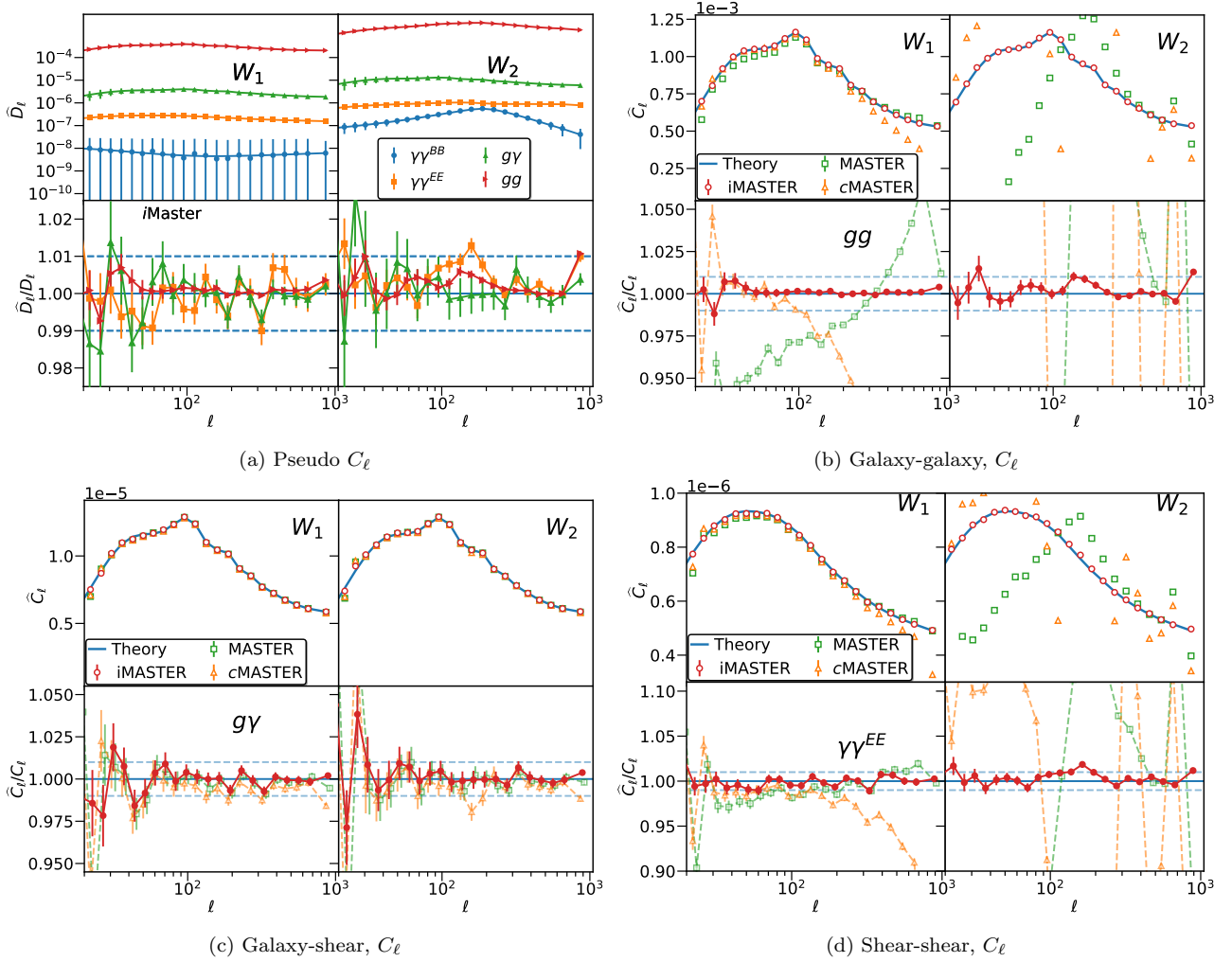


Figure 2. Comparisons of D_ℓ and C_ℓ of different observables, obtained using two different window functions, W_1 and W_2 (see appendix F). In the upper panel of each figure, the solid lines show the model predictions while the points represent the mean and the error on the mean from 1000 gaussian simulations. The lower panel show the ratio of simulations to the model predictions. a) Pseudo- C_ℓ power spectra, D_ℓ , for auto and cross correlations of galaxy positions and galaxy shear obtained using *i*MASTER algorithm. Model predictions agree with the simulations to better 1% after subtracting the noise. b-d) C_ℓ obtained by deconvolving power spectra using standard MASTER algorithm, *i*MASTER algorithm and the *c*MASTER algorithm. *i*MASTER gives unbiased power spectra (within 1% error) while MASTER and *c*MASTER algorithm gives biased results on scales where window has large power. The biases become worse as the complexity of the window increases. In $g\gamma$, where the window power spectra is small (window of galaxies and shear are uncorrelated) the biases in MASTER and *c*MASTER are small. The biases are largest in auto correlation with W_2 window which has large power out to high ℓ (see appendix F). As mentioned in [Alonso et al. \(2019\)](#), the *c*MASTER like results require convolving the theory power spectra with a coupling matrix in order to perform an unbiased comparison between theory and data (see also eq. (36)). The *i*MASTER requires no such corrections and the measurements can directly be compared with underlying binned theoretical model or the equivalent unbinned power spectra computed only at the effective scale ℓ_b of each bin.

tion),

$$B = \frac{U^T \text{Cov}^{-1}}{U^T \text{Cov}^{-1} U}, \quad (43)$$

where Cov is the covariance of the unbinned D_ℓ . U is $n_{bins} \times n_\ell$ matrix given by

$$U_{\ell_b, \ell} = \begin{cases} 1, \ell \in b \\ 0 \text{ otherwise.} \end{cases} \quad (44)$$

The optimal binning operator in eq. (43) depends on the unbinned covariance of the power spectra. While estimation of this covariance is expensive, it is naturally obtained in the intermediate steps when computing the analytical covari-

ances of binned power spectra. The binning operator can be obtained at the same time as computing covariance with little additional computing cost. B also depends on the particular power spectra being considered and hence each cross and auto correlation in a tomographic analysis will require different B . If such properties of B are not desirable, an approximation to B can be used where each ℓ is weighted by the effective number of modes (ignoring the effects of noise)

$$B_{\ell_b, \ell} \propto \begin{cases} \frac{2\ell+1}{(2\ell_b+1)\Delta\ell}, \ell \in b \\ 0 \text{ otherwise.} \end{cases} \quad (45)$$

Simulations and theory calculations shown in this work use the binning operators from eq. (45).

3.4 Window bias

In this section we discuss the response of the pseudo- C_ℓ estimator to the errors in estimating the window functions. We begin by noticing that the D_ℓ is symmetric in response to the window and the underlying over density field and therefore we can write (see appendix C):

$$D_\ell = M_{\ell,\ell''}^W W_{\ell''}, \quad (46)$$

where $M_{\ell,\ell''}^W$ is the response of D_ℓ to the window and depends on the C_ℓ . Relative error in D_ℓ due to errors in window power spectra can be written as

$$\frac{\partial \log D_\ell}{\partial W_{\ell''}} = \frac{1}{D_\ell} M_{\ell,\ell''}^W. \quad (47)$$

$\frac{1}{D_\ell} M_{\ell,\ell''}^W$ can be used to define the upper limits on the bias in window power spectra $\delta W_{\ell''}$ given an upper limit on the percentage bias D_ℓ that is acceptable.

Given the multiplicative and additive errors in the window as defined in section 2.2, we can also write the bias in D_ℓ as

$$\delta D_\ell = M_{\ell,\ell''}^W m_{\ell''} + a_\ell, \quad (48)$$

where $m_{\ell''}$ is the power spectra of the multiplicative bias ($m(\mathbf{x})W(\mathbf{x})$) and a_ℓ is the power spectra of the additive bias. It is important to note that multiplicative and additive biases do not necessarily have to be present together. For example, from eq. (21), it is possible that the estimated and true windows have the very similar power spectra but the two window are not very correlated. In such a case, window errors will behave like noise, resulting in additive bias a_ℓ but negligible multiplicative bias. Efficacy of window weighting will also be lost in such a case.

For window biases which may be described by eq. (25), under the assumption that the contaminant maps are not correlated, we can write (Ross et al. 2012; Leistedt et al. 2013; Elsner et al. 2017)

$$a_\ell = \sum_i \alpha_i^2 D_{i,\ell}, \quad (49)$$

$D_{i,\ell}$ is the power spectra of the contaminant maps. α_i can be estimated by cross correlating the estimated over density map (which includes systematics) with contaminant map as

$$\alpha_i = \frac{D_{i,\ell} \text{Cov}^{-1} \langle \hat{\delta}_g, W C_i \rangle_\ell}{D_{i,\ell} \text{Cov}^{-1} D_{i,\ell}}, \quad (50)$$

$$\text{Var}(\alpha_i) = \frac{1}{D_{i,\ell} \text{Cov}^{-1} D_{i,\ell}}. \quad (51)$$

$\langle \delta_g, W C_i \rangle_\ell$ is the cross power spectra between the over density map and the contaminant map. Cov is the joint covariance of the auto and cross correlations and eq. (51) denotes the variance of α_i . The method is only valid under the assumptions of linear expansion in eq. (25) and that the contaminant maps are independent. If the contaminant maps are not independent, one can use a PCA like method to project the contaminant maps into maps of orthogonal linear combinations which are uncorrelated and then define α_i and cross correlations over the new set of maps.

The cross correlation in eq. (50) is not sensitive to the m_ℓ as it shows up in the third order term, whose expectation is zero when window and the underlying overdensity field are uncorrelated. If the corrections from the above procedure are reliable and are applied to the window, it may reduce the effects of multiplicative bias as well.

For the case of multiplicative bias, fig. 3a shows the $\frac{1}{D_\ell} M_{\ell,\ell''}^W$ matrix. At low ℓ the matrix has nearly scale independent effects along the column, especially at $\ell = 0$. This accounts for the effects of the misestimation of the largest scales of the window, primarily sourced by the mask, and includes the effects of the mean of window or the f_{sky} factor. The diagonal of the matrix is sub-dominant at low ℓ but it increases as $\sim 2\ell + 1$, becoming large at high ℓ . Typically when modeling the window in power spectra such high ℓ effects are ignored. However, in fig. 3b, we see that this effect leads to rapidly increasing biases at higher ℓ , which dominate the information during the cosmological inference. Thus it is important to carefully model window out to high ℓ and properly account for any uncertainties in such modeling. Current modeling, e.g. Ross et al. (2012, 2020), uses HEALPIX maps with resolution of order $N_{\text{side}} = 512$, which may not be enough in the case of moderately complex windows even for $\ell_{\text{max}} \sim 1000$ (roughly similar to scale cuts in current weak lensing 3×2 analysis) and in the upcoming analysis such with LSST where we may wish to extend the analysis to $\ell_{\text{max}} \gtrsim 5000$, a much more careful characterization of the window will be needed.

To account for uncertainties in window effects, one can use some parametric function for m_ℓ which can be added to the D_ℓ model using eq. (48) and its parameters can be marginalized over. We can also use the analytical marginalization (Bridle et al. 2002), in which case the contributions from window uncertainties can be added to the covariance of the D_ℓ , and the additional contribution to the covariance can be written as

$$\text{Cov}^W(D_\ell, D_{\ell'}) \approx M^W m_\ell m_{\ell'}^T M^{W,T} + a_\ell a_{\ell'}^T, \quad (52)$$

where a_ℓ and its uncertainty can be obtained from eqs. (49)–(51). In general, if we have an estimation of the covariance of the window power spectra, W_ℓ , we can write

$$\text{Cov}^W(D_\ell, D_{\ell'}) \approx M^W \text{Cov}(W_\ell, W_{\ell'}) M^{W,T} + \text{Cov}(W_\ell, W_{\ell'}). \quad (53)$$

This expression is an approximation since a full covariance with the window and the over density field will require an expansion of 8-point function, which is tedious and computationally expensive even for the case of gaussian field. A detailed study of the window uncertainties in a realistic setting of LSS windows for the case of DESI survey will be presented in an upcoming work (Karim, Rezai & Singh in prep).

There are also cases where the window is well estimated but the multiplicative error can still have significant contributions to the covariance. One such case is when estimating the jackknife covariance, where each jackknife sample has a slightly different window and these seemingly minor differences can bias the covariance (Yu, Singh et al. in prep).

Finally, as discussed in section 2, it is also tempting to conclude that we can use cross correlations between different tracer/surveys to ‘self calibrate’ the effects of window.

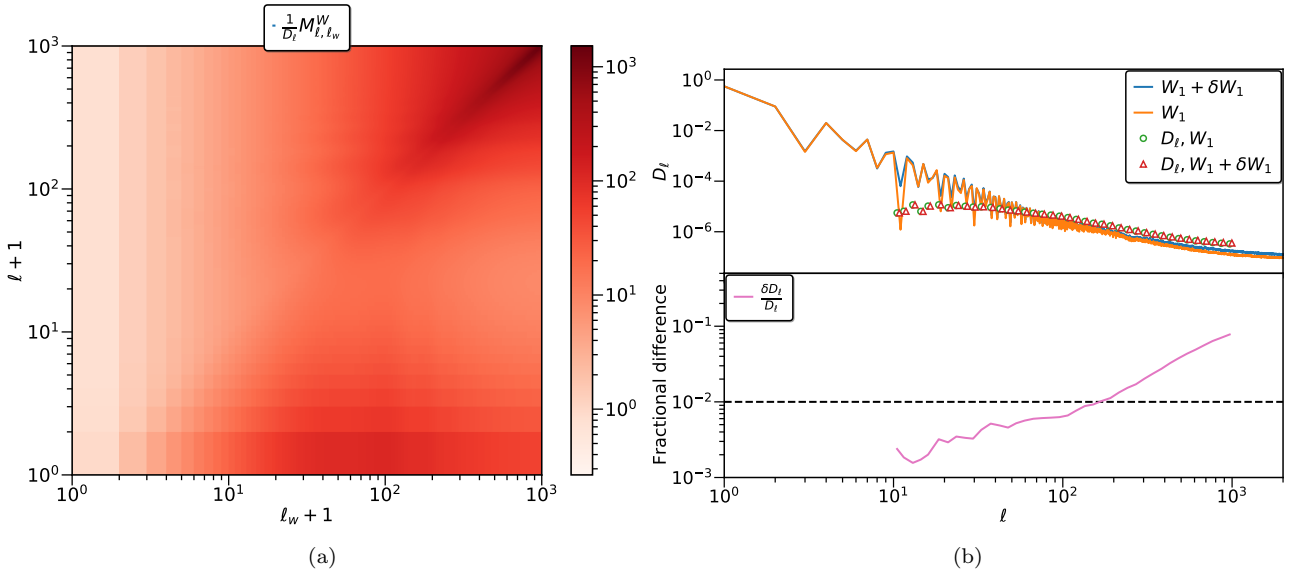


Figure 3. a) The matrix defined in eq. (47), which relates the errors in the window power spectra, δW_ℓ to the relative errors in the D_ℓ , i.e. $\frac{\delta D_\ell}{D_\ell} = \left(\frac{1}{D_\ell} M^W\right) \delta W_\ell$. Note that ℓ values are shifted by 1 to show the $\ell = 0$ column which relates the f_{sky} error to errors in D_ℓ . At high ℓ the matrix has strong values around the diagonal which increases the relative sensitivity of D_ℓ to the window power spectra. b) Demonstration of the multiplicative bias introduced in D_ℓ by errors in W_ℓ (there is no additive bias in this figure). In the upper panel, solid orange line shows the default window while blue line shows the perturbed window. Green circles and red triangles show the D_ℓ obtained using these windows and the lower panel shows the fractional bias introduced in D_ℓ . Here the window was perturbed by simply adding a white noise with $N_\ell \sim W_{\ell=500}$ power spectra ($N_{\ell < 10} = 0$ and $\delta f_{\text{sky}} = 0$ by construction). W_1 refers to the realistic galaxy shear like window (see appendix F).

However, this in general does not work unless the windows between tracer/surveys are perfectly correlated. An example of such an effect can be observed on figs. 1 and 2, where galaxies and shear have uncorrelated window by design and hence the cross correlation, $g\gamma$, is almost completely free of the window effects except for the very large scales (low ℓ), where windows are partially correlated due to the mask effects. Thus it is in general not possible to use the cross correlation, $g\gamma$, to understand the window effects in auto correlations, gg and $\gamma\gamma$ in our case.

4 CORRELATION FUNCTIONS

In this section we discuss the two point function measurements in the configuration space, namely the correlation functions. We begin with brief introduction of correlation functions and will discuss the estimators, effects of windows, the methods to apply scale cuts and the generalization of the *i*MASTER algorithm to reconstruct the power spectra from the correlation functions.

The curved sky correlation function can be written as the Hankel transform of the power spectra,

$$\xi(\theta) = \sum_{\ell} \frac{2\ell + 1}{4\pi} s_1 d_{\ell, s_2}(\theta) C_\ell = \mathcal{H}_{\theta, \ell} C_\ell, \quad (54)$$

where $s_1 d_{\ell, s_2}$ is the wigner-d matrix, with s_1, s_2 being the spins of tracers being correlated and in the second equality we have written the sum as a matrix multiplication, with \mathcal{H} being the Hankel transform operator. The sum is over all ℓ and therefore computing ξ to an arbitrary accuracy can be expensive. Fortunately, C_ℓ drops with ℓ , $C_\ell \sim \ell^{-2}$, therefore very high ℓ modes contribute very little and the summation

can be truncated at $\ell \sim a\pi/\theta$, where $a \sim 5 - 10$ is a suitably chosen constant. We will see in section 4.2 that one can also work with the binned quantities similar to the discussion for the pseudo- C_ℓ to further speed up the calculation. But first we discuss the estimator used to measure the correlation functions.

4.1 Landy-Szalay estimator

The correlation functions measure the excess probability of finding galaxies around other galaxies at a given separation. These are measured by counting the excess number of pairs of galaxies at a given separation relative to a distribution of randoms. The commonly employed Landy-Szalay estimator (Landy & Szalay 1993) is given by

$$\xi(\theta_b) = \frac{B_\theta(DD - DR - RD + RR)}{B_\theta RR}, \quad (55)$$

where B_θ is the binning operator, D denotes the galaxies, R denotes the randoms that correspond to the galaxy sample and different two points, e.g. $B_\theta DD$, denote the count of auto and cross pairs of galaxies and randoms with separation θ that falls within the bin θ_b . It can be shown that when randoms follow the window function, LS is an optimal estimator to compute the two point correlation functions (Landy & Szalay 1993; Singh et al. 2017).

We now show that the LS estimator is equivalent to correlating the over density maps as defined in section 2. The pairs counts can be written as integral over the galaxy density field, i.e.

$$DD(\theta) = \int_{\theta'} n_g(\theta') n_g(\theta' + \theta). \quad (56)$$

$\int_{\theta'} = \int d\phi' d\theta' \sin(\theta')$ is the integral over the volume element in θ' . From this we can show that the eq. (55) is equivalent to

$$\xi(\theta_b) = \frac{B_\theta \int_{\theta'} (n_g(\theta') - n_R(\theta')) (n_g(\theta' + \theta) - n_R(\theta' + \theta))}{B_\theta \int_{\theta'} n_R(\theta') n_R(\theta' + \theta)}. \quad (57)$$

Using the definition of δ from eq. (3) and (7), we get

$$\xi(\theta_b) = \frac{B_\theta \int_{\theta'} W(\theta') \delta_g(\theta') W(\theta' + \theta) \delta_g(\theta' + \theta)}{B_\theta \xi_W(\theta)}, \quad (58)$$

where $\xi_W(\theta)$ is the correlation function of window. From eq. (58), the LS estimator is same as correlating the over-density field, as long as the pixel size of the map is small enough to measure the minimum scale of interest. Computing correlation functions via pixels can be cheaper when we have more than one galaxy (or more accurately, one random point) per pixel on average. Further gains can also be made by taking advantage of the regularized nature of the pixel grid. Since use of randoms is simply a monte-carlo method to account for window effects in the estimator, direct correlation of maps will also be free from additional noise introduced by the randoms.

As discussed in section 2, when computing correlation functions from galaxy catalogs, usually one of following two approaches is adopted. In the first case, randoms are uniformly distributed on the sky and the galaxies are weighted by $1/W(\theta')$. This approach is commonly used (e.g. Ross et al. 2012, 2020; Alam et al. 2016; Elvin-Poole et al. 2018) and is equivalent to using the over density map as defined in eq. (5). In the second method, the random are weighted by the window, i.e. $n_R(\theta') = \bar{n}_g W(\theta')$ and galaxies are assigned uniform weight. This approach is equivalent to correlating the maps as defined in eq. (3). In terms of optimality, same arguments as presented in section 2 applies to the question of weighing galaxies vs randoms, i.e. in general it is better to apply weights to randoms.

It is also worth noting that the $B_\theta \xi_W(\theta)$ term (the RR term) in the denominator is not strictly necessary if the window effects are properly accounted for in the modeling. The use of this term in the estimator can also lead to the sub-optimal results as it up-weights the noisy modes where $B_\theta \xi_W(\theta)$ is low. It can be more optimal to instead use a simple normalization constant, e.g. $A_W = f_{\text{sky}}$ (or $A_W = 1$). In such a case, it can be easily shown using the equations in appendix E1 (replace $w(\theta)$ with ξ_W) that the correlation function and the pseudo- C_ℓ estimators are identical when the measurements are performed over the full range of scales, $\theta \in [0, \pi]$ and $\ell \in [0, \infty]$. In the following section we relax this condition and study the relations between correlation functions and power spectra over a limited range of scales.

4.2 iMASTER for correlation functions

In the previous section, we have studied the correlation function estimators and showed their equivalence to the power spectra estimators. Now we will study the relations between correlation functions and power spectra for the practical cases where the measurements and the models are defined over a limited range of scales. We will generalize the iMASTER algorithm to reconstruct power spectra from the

correlation function measurements done over a limited θ range and will also derive the expressions for properly implementing scale cuts on the correlation functions when the model is defined in Fourier space.

From eq. (58) and appendix D, the correlation function for a windowed field is given by

$$\xi(\theta_b) = \frac{B_\theta \xi_W(\theta) \mathcal{H}_{\theta, \ell} C_\ell}{B_\theta \xi_W(\theta)}. \quad (59)$$

We can use the trick from section 3.3 and bin both ξ and C_ℓ

$$\xi(\theta_b) = \frac{1}{B_\theta \xi_W(\theta)} B_\theta \xi_W(\theta) \mathcal{H}_{\theta, \ell} B_C^{-1} B_C C_\ell, \quad (60)$$

where B_θ is binning operator in θ , acting on ξ and B_C is the binning operator in ℓ , acting on C_ℓ . Therefore we can write the operation in terms of binned quantities, where the binned Hankel transform is given by

$$\mathcal{H}_{\theta_b, \ell_b} = \frac{1}{B_\theta \xi_W(\theta)} B_\theta \xi_W(\theta) \mathcal{H}_{\theta, \ell} B_C^{-1}. \quad (61)$$

As discussed in previous section 4.1, the $B_\theta \xi_W(\theta)$ term in the denominator of eq. (59) can be replaced with a constant A_W , in which case the binned Hankel transform changes to,

$$\mathcal{H}_{\theta_b, \ell_b} = \frac{1}{A_W} B_\theta \xi_W(\theta) \mathcal{H}_{\theta, \ell} B_C^{-1}. \quad (62)$$

θ_b is the effective θ at which the correlation function is measured and is given by

$$\theta_b = \frac{B_\theta (\theta \xi_W(\theta) \xi(\theta))}{B_\theta (\xi_W(\theta) \xi(\theta))}. \quad (63)$$

An aside, $\mathcal{H}_{\theta_b, \ell_b}$ can be used to transform C_ℓ to binned correlation function in $O(N_{\text{bin}}^2)$ time instead of $O(N_\ell N_\theta)$, where $N_\theta \gg N_{\text{bin}}$ thereby speeding up the calculations without compromising the accuracy.

Finally, we can invert Hankel transform to reconstruct the binned power spectra as

$$C_{\ell_b} = \mathcal{H}_{\ell_b, \theta_b}^{-1} \xi(\theta_b). \quad (64)$$

In general, in the presence of scale cuts in θ , the inversion of $\mathcal{H}_{\ell_b, \theta_b}$ can be unstable. It is better to define inverse of $\mathcal{H}_{\ell_b, \theta_b}$ from the definition of the inverse transform, where

$$C_\ell = 2\pi \int d\theta \sin(\theta)_{s_1} d\ell_{s_2}(\theta) \xi(\theta). \quad (65)$$

Replacing the integral with sum over discrete values of θ , we can write

$$\mathcal{H}_{\ell, \theta}^{-1} = 2\pi \Delta \theta \sin(\theta)_{s_1} d\ell_{s_2}(\theta), \quad (66)$$

which can then be binned to obtain

$$\mathcal{H}_{\ell_b, \theta_b}^{-1} = B_C \mathcal{H}_{\ell, \theta}^{-1} B_\theta^{-1}. \quad (67)$$

Notice that in this process we are reconstructing the true power spectra and not the pseudo- C_ℓ as long as the correlation functions are measured over the full range, $\theta \in [0, \pi]$. The effects of the survey window are absorbed in the $\mathcal{H}_{\ell_b, \theta_b}^{-1}$ via the B_θ^{-1} operation. B_θ^{-1} is defined similar to eq. (39) using the ratio $\xi(\theta)/\xi(\theta_b)$.

In practice, the correlation functions are usually measured over a limited range of scales, in which case we define

$$\xi_{\text{cut}}(\theta) = \xi(\theta) w(\theta), \quad (68)$$

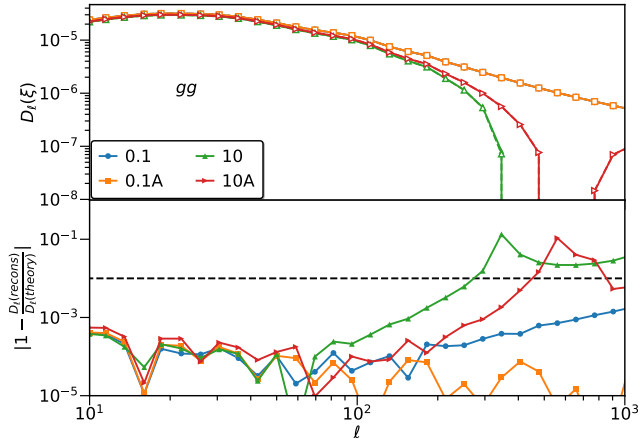


Figure 4. Pseudo- C_ℓ power spectra obtained after inverse Hankel transform of the correlation function, ξ . ξ was computed over the range $[0.01, 600]$ arcminutes. For blue and green points, I apply a hard cut on ξ and 0.1 and 10 arcminutes respectively. Solid lines show the C'_ℓ converted using coupling matrix, $M_{\ell, \ell'}$. Orange and Red point show the attempt to reduce the complexity of the coupling matrix by apodizing the $w(\theta)$ by multiplying its Hankel transform w_ℓ with a function that smoothly goes from one to zero in the range, $\ell \in [100, 1000]$. While apodization helps, it does so by including information from lower θ than the original θ_{cut} and in practice one may need fairly strong apodization if ξ is computed over narrow θ range.

where $w(\theta)$ is a weight function (usually a top hat function with the limits of $\theta_{\min}, \theta_{\max}$) that applies the scale cuts. Inverting ξ_{cut} , we will get

$$\mathcal{H}_{\ell_b, \theta_b}^{-1} \xi_{\text{cut}}(\theta) = M_{\ell_b, \ell'_b} C_{\ell'_b}, \quad (69)$$

where M_{ℓ_b, ℓ'_b} is the coupling matrix as defined in eq. (27) and eq (41), this time with $w(\theta)$ acting as window (see appendix E for derivation). Note that when θ range is small, the coupling matrix can be rather broad in which case separate binning operators on B_D and B_C may be required similar to eq (41).

In figure 4, we see the D_ℓ obtained by the inverse Hankel transform of the correlation function. For a wide range, $\theta \in [0.1, 600]$ arcminutes, the D_ℓ from inverse Hankel transform of correlation function and from convolving C_ℓ are consistent. However, for larger $\theta_{\min} = 10$ arcminutes, the results from convolving C_ℓ are biased. This is because the coupling matrix $M_{\ell, \ell'}$ is very broad and the range $\ell \in [0, 3000]$ used here for C_ℓ calculations is not enough. This is demonstration of the case where we require $\ell', \ell'' \gg \ell$ when computing the coupling matrix (see discussion after eq. (27)). The figure also shows an attempt to reduce the complexity of the coupling matrix by apodizing the scale cut window $w(\theta)$. Here a simple procedure was adopted where the w_ℓ is multiplied with a cosine function which goes from one to zero for $\ell \in [100, 1000]$ and then w_ℓ is transformed back into $w(\theta)$. This apodized window effectively brings back some power from $\theta < 10$ arcminutes and helps in partially reducing the bias. In practical applications, one will have to experiment with a few different apodization schemes depending on the measurements being performed and scales being used to obtain good results.

From eq. (69), the power spectra can be reconstructed

from correlation functions as

$$C_{\ell'_b} = M_{\ell'_b, \ell_b}^{-1} \mathcal{H}_{\ell_b, \theta_b}^{-1} \xi_{\text{cut}}(\theta_b) = \mathcal{M}_{\ell'_b, \theta_b} \xi_{\text{cut}}(\theta_b), \quad (70)$$

where we defined

$$\mathcal{M}_{\ell'_b, \theta_b} = M_{\ell'_b, \ell_b}^{-1} \mathcal{H}_{\ell_b, \theta_b}^{-1}. \quad (71)$$

The covariance of reconstructed power spectra is

$$\text{Cov}(C_{\ell_1}, C_{\ell_2}) = \mathcal{M}_{\ell_1, \theta_1} \text{Cov}(\xi_{\theta_1}, \xi_{\theta_2}) \mathcal{M}_{\ell_2, \theta_2}^T. \quad (72)$$

Note that unlike existing methods in the literature, e.g. Joachimi et al. (2021), the *i*MASTER method we discuss here returns the unbiased C_ℓ power spectra at the effective bin centers, ℓ_b and removes any effects of mode mixing from the correlation function measurements done over a limited range of scales. The method also accounts for the window effects which has not been done before in literature to the best of my knowledge. As in section 3.3, the results from eq. (70) and (78) can directly be compared with the model C_ℓ predictions and do not require any additional operations such as binning or any corrections to be applied.

In fig. 5, we see the comparison of the reconstructed power spectra from both correlation function and the direct pseudo- C_ℓ power spectra (all calculations are analytical). Correlation functions are computed over a wide range, $\theta \in [0.01, 1200]$ arcminutes, to lower the complexity of the coupling matrix. Both correlation functions and pseudo- C_ℓ give consistent results to well within 1%. The right panel of the figure also shows the comparison of the signal to noise ratio (S/N) as function of ℓ_{\max} . To obtain S/N of reconstructed C_ℓ , we inverted the analytical gaussian covariances of pseudo- C_ℓ (Efstathiou 2004) and correlation functions (see appendix A of Singh et al. 2017) using the relation in eq. (72). The S/N is defined as

$$S/N = \sqrt{C_\ell \text{Cov}^{-1} C_\ell}. \quad (73)$$

Recently there has been some discussion about the apparent discrepancies or low correlation in the cosmological analysis from correlation functions and power spectra (e.g. Doux et al. 2021; Hamana et al. 2020). These discrepancies are known to be caused primarily by effects of the scale cuts imposed on the estimators, in addition to some small effects caused by approximations made in covariances and the estimators (see section 4.1). From eq. (D9) and appendix E1, it can be shown that when full range of scales is used, the correlation function and power spectra have same information, i.e. up to the normalization factor of window in correlation functions (the RR term in the denominator), the correlation function and pseudo- C_ℓ are the same. Because of the impact of scale cuts, it is sometimes claimed that correlation functions and power spectra provide complementary information. This is true in the technical sense as the coupling matrix becomes complex with scale cuts in θ (see fig. 4), leading to mixing of information from larger ℓ range and the information from different ℓ modes is complementary (assuming they are independent). However, such ‘complementarity’ is not desirable if we do not have a good model for the subset of ℓ modes (which is usually the motivation for scale cuts). Mixing of information from such scales only complicates the interpretation of the full posteriors from the analysis, even if the analysis is shown to be ‘unbiased’ under some tests. To further understand the potential implications, consider the fact that the size of scatter shown in fig.

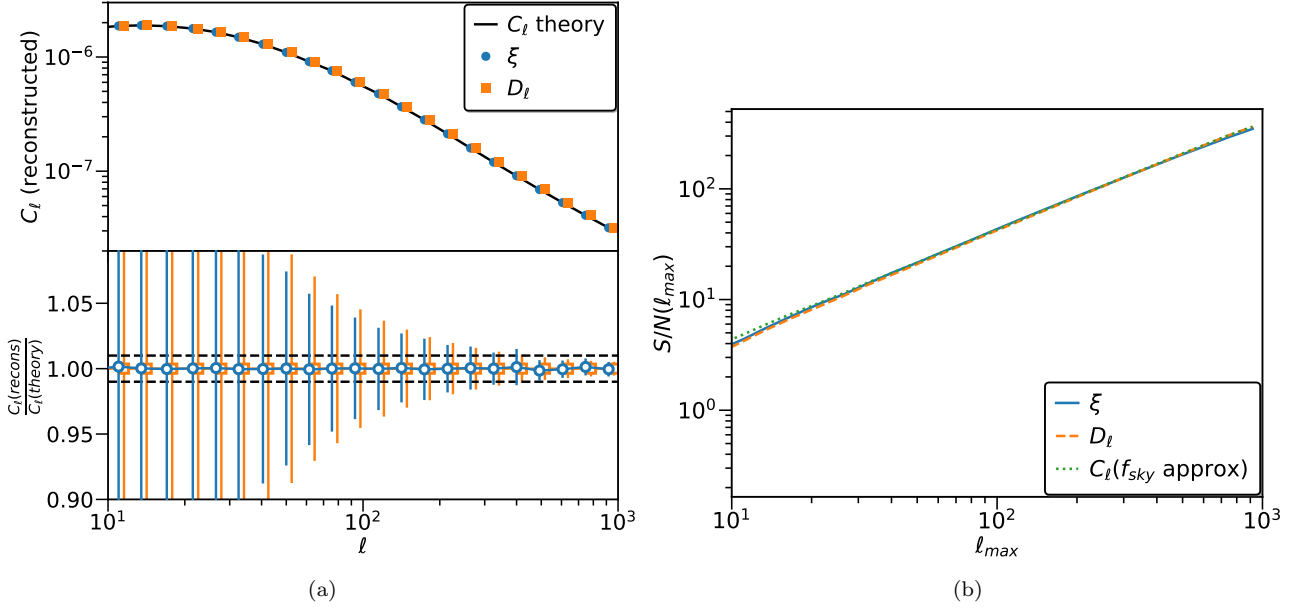


Figure 5. a) Power spectra reconstructed from binned correlation function (blue points) with $\theta \in [0.01, 1200]$ arcminutes and the pseudo- C_ℓ power spectra from section 3.3. This plot uses W_1 window (see appendix F). Lower panel shows the ratio with the input C_ℓ , with errorbars from the analytical covariance and one percent deviations marked by dashed black lines. Note that the C_ℓ reconstructed from ξ and D_ℓ are not perfectly correlated due to the impact of limited θ range and the window correction term in the correlation function estimator (see discussion in section 4.1). Different assumptions made in covariance calculations and the numerical noise in converting them also have some impact on the errorbars shown and thus this comparison should be taken as approximate. b) Signal to noise ratio (S/N) as function of ℓ_{\max} cut off for the reconstructed power spectra in a). Also shown in the S/N for C_ℓ with a diagonal covariance with same f_{sky} . For $\ell_{\max} > 100$, all three curves agree to within $\sim \pm 5\%$.

17 of Hamana et al. (2020) and fig. 9 of Doux et al. (2021) is comparable to the statistical uncertainties on parameters and to the magnitude of tensions observed between some of the weak lensing measurements and the predictions from Planck cosmology.

In general, if possible, one should keep data and model in the same space to avoid the complexities of transforming to the Fourier counterpart. Fig. 5 shows that when treated consistently, the correlation functions and power spectra carry similar information and the differences are primarily driven by scale cuts, which we need to implement carefully. We have addressed the implications of scale cuts imposed on correlation functions when reconstructing the power spectra and we will address the inverse of this process, namely the impact on correlation function when the scale cuts are imposed on the model in the Fourier space in section 4.2.2. Before that, we now address the issue of reconstructing lensing E/B modes from the cosmic shear correlation functions.

4.2.1 E/B mode reconstruction

For cosmic shear measurements, we typically measure two sets of correlation functions, ξ_+ and ξ_- , which can be written in terms of the underlying EE and BB power spectra as

$$\xi_{\pm}(\theta_b) = H_{\pm, \theta_b, \ell_b}(C_\ell^{EE} \pm C_\ell^{BB}), \quad (74)$$

where $H_{\pm, \theta_b, \ell_b}$ are Hankel transform operators as defined in eq (67) with spin-2 wigner-d matrices, ${}_2d_{\ell, \pm 2}$.

Using eq. (70) we can also do a clean E/B mode separation for the case of cosmic shear, by converting ξ_{\pm} to

pseudo- C_ℓ as

$$D_{\ell_b}^{\pm} = \mathcal{H}_{\pm, \ell_b, \theta_b}^{-1} \xi_{\pm}(\theta_b). \quad (75)$$

Here we assume that the ξ_{\pm} are measured over the same θ range. Now we can obtain E/B pseudo-power spectra as

$$D_{\ell_b}^{EE} = \frac{1}{2}(D_{\ell_b}^{+} + D_{\ell_b}^{-}) \quad (76)$$

$$D_{\ell_b}^{BB} = \frac{1}{2}(D_{\ell_b}^{+} - D_{\ell_b}^{-}). \quad (77)$$

$D_{\ell_b}^{EE, BB}$ and the coupling matrices are defined in section 3.1. From $D_{\ell_b}^{EE, BB}$, we can reconstruct the underlying E/B power spectra as

$$\hat{C}_{\ell_b}^{EE} = (M_b^{+EE})^{-1} \hat{D}_{\ell_b}^{EE} - (M_b^{+EE})^{-1} M_b^{-BB} C_{\ell_b}^{BB} \quad (78)$$

$$\hat{C}_{\ell_b}^{BB} = (M_b^{+BB})^{-1} \hat{D}_{\ell_b}^{BB} - (M_b^{+BB})^{-1} M_b^{-EE} C_{\ell_b}^{EE}. \quad (79)$$

M_b are binned coupling matrices, with the superscript, e.g. $+EE$, referring to the power spectra used in defining the B^{-1} operator. In eq. (78) and (79), we have also made a distinction between the quantities measured from data, denoted with $\hat{\cdot}$, and the ones estimated from theory. We are using the model $C_{\ell_b}^{EE, BB}$ to subtract out the leakage contribution of the form, $M^{-} C_{\ell_b}$. This is likely to be sufficient for most applications as $(M^{+})^{-1} M^{-}$ is typically small ($\lesssim 10^{-2}$) for broad windows. When noise is sub-dominant, it may be desirable to replace the C_ℓ from model with the ones from data in order to cancel sample variance, e.g. in the case where we are attempting to detect and reconstruct small B mode power spectra. Under such a scenario, we can use an iterative method where the initial estimates of $\hat{C}_{\ell_b}^{EE, BB}$ from

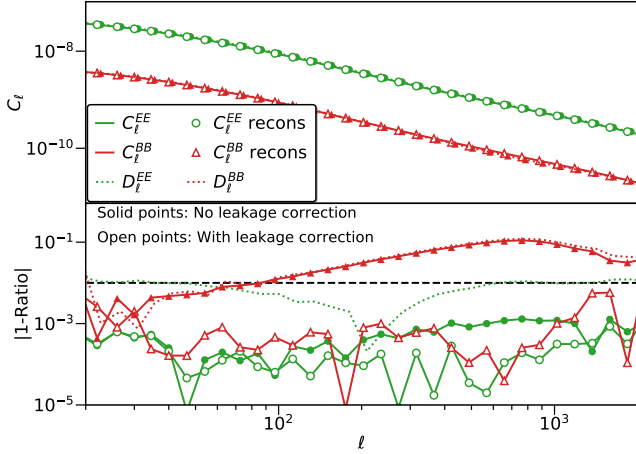


Figure 6. Demonstration of shear EE and BB power spectra reconstruction from ξ_{\pm} correlation functions via the *i*MASTER algorithm. *Upper panel:* Solid lines show the true underlying power spectra, where we assumed $C_{\ell}^{BB} = 0.1C_{\ell}^{EE}$ for this demonstration. Dotted lines show the pseudo-power spectra constructed via inverse Hankel transform, solid points show reconstructed power spectra from D_{ℓ} while setting leakage terms $M^{-}C_{\ell}^{EE,BB} = 0$ (see eq. (78) and (79)) and open points show the results when correct $M^{-}C_{\ell}^{EE,BB}$ is used. *Lower panel:* Fractional errors in different curves with respect to the true $C_{\ell}^{EE,BB}$. Both leakage and the window effects lead to errors of order few percent which are removed when using correct expressions in eq. (78) and (79). The residuals errors are primarily from the limited θ and ℓ range used in the tests and can be reduced further by expanding these ranges.

eq. (78) and (79) can be used to replace theory $C_{\ell_b}^{EE,BB}$ in the next iteration. Only few such iteration will be required as the excess sample variance effects from leakage ($\hat{C}_{\ell} - C_{\ell}$) scale down as $[(M^{+})^{-1}M_{-}]$. We have also neglected the possibility of reconstructing power spectra from terms involving M^{-} terms, i.e., reconstructing $\hat{C}_{\ell_b}^{EE,BB}$ from $\hat{D}_{\ell_b}^{BB,EE}$ (EE from BB and BB from EE). In such reconstruction the noise scales as $[(M^{-})^{-1}M_{+}]$, which is very large ($\gtrsim 10^2$) when window is broad (narrow in ℓ space) and thus we do not expect to gain much in terms of signal to noise of the overall $\hat{C}_{\ell_b}^{EE,BB}$.

Fig. 6 demonstrates the reconstruction of the EE and BB power spectra reconstructed from ξ_{\pm} correlation function. Here we assumed $C_{\ell}^{BB} = 0.1C_{\ell}^{EE}$ to demonstrate the steps in the reconstruction (we assume $C_{\ell}^{BB} = 0$ in rest of the paper). The pseudo- C_{ℓ} obtained by inverse Hankel transform of correlation functions are biased by few percent as expected. Reconstructing the power spectra without the correction for leakage, i.e. we set $M^{-}C_{\ell}^{EE,BB} = 0$, also leads to biased results, especially for the B mode power spectra which is smaller and hence more sensitive to these biases. Using expressions in eq. (78) and (79) allow us to obtain unbiased results to better 1% accuracy (note that this accuracy depends on the choice of scale cuts on ξ_{\pm} and the ℓ_{\max} of coupling matrix. Smaller θ range in correlation functions will require larger ℓ_{\max} for same accuracy). Setting $M^{-}C_{\ell}^{EE,BB} = 0$ initially and then adopting the iterative procedure as discussed above converges to same unbiased results in two iterations after which there are no further improvement (not shown).

4.2.2 Model cuts in Fourier space

Many of the cosmological models are written and validated in the Fourier space and thus have a well defined cuts in the Fourier space based on their scales of validity. This implies truncation in the summation in eq. (54). Similar to the issues we addressed in the case of power spectra, the truncation in the Fourier counterpart should result in a convolution on the correlation functions of the form (see appendix E for derivation),

$$\xi_{\ell-\text{cut}}(\theta) = \mathcal{H}_{\theta,\ell} C_{\ell} b_{\ell} = b(\theta, \theta') \otimes \xi(\theta'), \quad (80)$$

where b_{ℓ} is the truncation function in the Fourier space and in the second equation we wrote the computed correlation function as a convolution between true underlying correlation function and the Hankel transform of b_{ℓ} , given by (see appendix E)

$$b(\theta, \theta') = \sum_{\ell} b_{\ell} \frac{2\ell+1}{4\pi} s_1 Y_{\ell,s_2}(\theta) s_1 Y_{\ell,s_2}(\theta'). \quad (81)$$

Therefore in the case of a theory cut off defined in Fourier space, we can simply convolve the measured correlation function with the $b(\theta, \theta')$ to impose the ‘scale cuts’ before running the inference chain. Using our binning trick from previous sections, we can define the binned version of the coupling matrix,

$$b(\theta_b, \theta'_b) = B_{\theta} b(\theta, \theta') B_{\theta}^{-1}. \quad (82)$$

Also note that b_{ℓ} is operationally same as an isotropic pixel/beam smoothing applied on over density maps with the beam function given by $\sqrt{b_{\ell}}$. Thus this method can be used to account for such smoothing effects as well. We can also account for correct factors of b_{ℓ} in the covariance and cross covariance calculations by considering each tracer to be smoothed by its own ‘beam’ given by $\sqrt{b_{\ell}}$, which can be different for different tracers (also remember that shot noise in covariance will no longer scale as $1/N_{\text{pairs}}$ after smoothing).

While b_{ℓ} is typically chosen to be top hat function, it can lead to convolution over rather large scales in θ . A choice of with more compact $b(\theta, \theta')$ can be given by a function that drops more smoothly from one to zero, such as

$$b_{\ell,\cos} = \begin{cases} 1, & \ell \leq \ell_{\text{cut,min}} \\ \cos\left(\frac{\pi}{2} \frac{\ell - \ell_{\text{cut,min}}}{\ell_{\text{cut,max}} - \ell_{\text{cut,min}}}\right), & \ell_{\text{cut,min}} < \ell < \ell_{\text{cut,max}} \\ 0 & \ell \geq \ell_{\text{cut,max}} \end{cases}, \quad (83)$$

where $b_{\ell,\cos}$ use a cosine function to smoothly truncate the power spectra to zero between $\ell_{\text{cut,max}} - \ell_{\text{cut,min}}$. A larger separation between $\ell_{\text{cut,max}}$ and $\ell_{\text{cut,min}}$ will lead to narrower convolution in θ space.

More frequently, the cutoff in theoretical models are defined in the comoving (k) space, in which case the b_{ℓ} can be written as

$$b_{\ell,k-\text{cut}} = \frac{C_{\ell,k-\text{cut}}}{C_{\ell}}, \quad (84)$$

where $C_{\ell,k-\text{cut}}$ is computed with cut off in k and C_{ℓ} is true underlying power spectra without any cutoff. This requires us to have some estimate of C_{ℓ} and in practice it will likely be better to use some combination of $b_{\ell,k-\text{cut}}$ and $b_{\ell,\cos}$, i.e. $b_{\ell,\cos} \times b_{\ell,k-\text{cut}}$, for more accurate results.

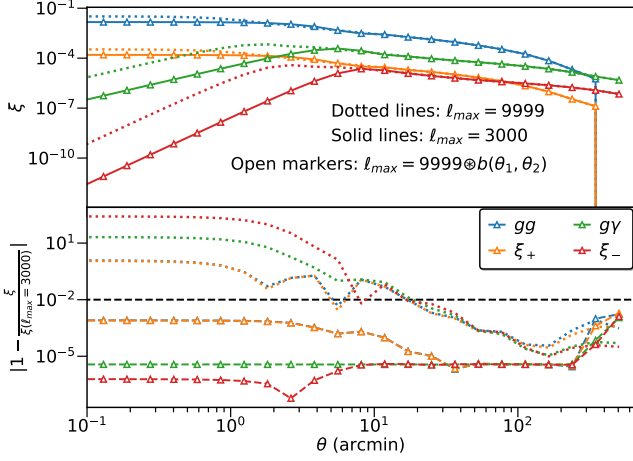


Figure 7. Comparison of correlation functions obtained with different ℓ cuts for auto and cross correlations of galaxies and shear. Dotted lines show ξ obtained with $\ell_{\max} = 10^4$, while solid lines show the case with a theory cut applied using b_ℓ , with $\ell_{\max} = 3000$. The open points show the results obtained by convolving ξ obtained using $\ell_{\max} = 10^4$ with the $b(\theta, \theta')$ to reproduce the ξ with $\ell_{\max} = 3000$ cut. The lower panel shows the fractional differences. Dashed lines are for the ratio of ξ s with $\ell_{\max} = 10^4$ and $\ell_{\max} = 3000$ while dashed lines with open markers show the same, using ξ with $\ell_{\max} = 10^4$ and convolved with $b(\theta, \theta')$.

Fig. 7 shows the effects of convolving the correlation function with $b(\theta, \theta')$ to account for the effects of the scale scale cuts imposed on the model. After convolution, the correlation function with high ℓ_{\max} agrees to much better than 1% with the correlation function with lower ℓ_{\max} cut.

For the case of galaxy-shear cross correlations, it is also worth comparing the effects of eq. (80) to the Υ estimator suggested by Baldauf et al. (2010). The Υ estimator is relevant for applying scale cuts when the model and hence the scale cuts are described in the real space. Eq. (80) should be used when the model and its cuts are described in the Fourier space.

We can also write convolution operators for the case of flat-sky approximation, for both projected and three dimensional (spectroscopic) statistics (Baddour 2014)

$$b(\theta, \theta')_{\text{flat sky}} = \int d\ell b_\ell J_n(\ell\theta) J_n(\ell\theta'), \quad (85)$$

$$b(r, r') = \int dk k^2 b(k) j_n(kr) j_n(kr'). \quad (86)$$

4.2.3 Hybrid cuts

In practice, both model and data may have scale cuts applied which may complicate the analysis when data and model are in separate spaces. For example, we may have correlation function measurements, with some scale cuts due to systematics such as blending or fiber collisions while the model is defined in the Fourier counterpart, i.e. power spectra. In such a case, eq. (80) modifies to

$$\xi_{\ell, \theta - \text{cut}}(\theta) = b(\theta, \theta') \otimes \xi(\theta') w(\theta') = \mathcal{H}_{\theta, \ell} D_\ell b_\ell, \quad (87)$$

where in the second part of the equation we now have pseudo- C_ℓ instead of C_ℓ .

In such a case, it is easiest to work with the reconstructed power spectra via iMASTER, as in eq. (70) or in eq. (35) (with M from eq. (41)) if one is working with the pseudo- C_ℓ measurements. For E/B power spectra, the procedure in section 4.2.1 should be followed.

It can also be computationally efficient to combine the correlation function and pseudo- C_ℓ estimators for the reconstruction of power spectra on all scales. The pair counting correlation functions estimators are fast to implement at small scales (total number of pairs is small) while the pseudo- C_ℓ estimators are faster at large scales (Fourier transforms can be computed on coarser grids/maps). Reconstructing C_ℓ from both estimators and then combining them with minimum variance weighting can result in faster reconstruction of C_ℓ over a broad range of modes.

4.3 Window errors

As discussed in section 4.1, the correlation function measured using the LS estimator is given by

$$\xi(\theta_b) \approx \frac{B_\theta \xi_W(\theta) \xi(\theta)}{B_\theta \xi_W(\theta)}, \quad (88)$$

where $\xi_W(\theta)$ is the correlation function of the window. Note that the binning operation is applied separately to the numerator and the denominator. If $\xi_W(\theta)$ has a strong gradient within the bin, it can introduce a bias, namely that the effective scale of the measurement θ_b (eq. (63)) will be different from the bin center computed without accounting for the window effect.

Since the Landy-Szalay estimator uses the estimated window (randoms follow the estimated window function), which maybe different from the true underlying window, correlation functions also suffer from the window bias. The numerator of eq. (88) has the correlation function of the true window (W) while the denominator has the correlation function of the estimated window (\hat{W}). In presence of these biases we get

$$\xi(\theta_b) = \frac{B_\theta \xi_W(\theta) \xi(\theta)}{B_\theta (1 + m_\theta(\theta)) \xi_W(\theta)} + a(\theta_b), \quad (89)$$

where $a(\theta_b)$ is the correlation function of the additive bias and we introduced m_θ to refer to the multiplicative bias in the correlation function of the window. As in the power spectra, $a(\theta_b)$ is easily accounted for by using the correlations method (e.g. Ross et al. 2012), but $m(\theta)$ is usually harder to estimate and can introduce significant biases, especially if it has a strong scale dependence. Since correlation functions and pseudo- C_ℓ are same, we can use the same methods as described in section 3.4 to understand these window biases and add corrections terms to the data/model or to the covariance.

5 CONCLUSION

In this paper we reviewed the formalism for the measurement and modeling of two point functions of the cosmological tracers, starting from the process of making maps from the catalogs to the measurements of the power spectra and the correlation functions and addressed several of the issues related to the importance of survey window, biases in its

Algorithm 1 *i*MASTER for power spectra

Input: Measured power spectra \hat{D}_ℓ ; Window power spectra \hat{W}_ℓ ; Model power spectra C_ℓ , N_ℓ ; Binning operators B_D , B_C .

1. Subtract the noise from \hat{D}_ℓ , i.e. $\hat{D}_\ell = \hat{D}_\ell - N_\ell$.
2. Bin \hat{D}_ℓ , to obtain $\hat{D}_{\ell_b} = B_D \hat{D}_\ell$.
3. Bin C_ℓ , to obtain $C_{\ell'_b} = B_C \hat{C}_{\ell'}$.
4. Obtain ℓ'_b , eq. (40).
5. Obtain B_C^{-1} , eq. (39).
6. Compute the coupling matrices, $M_{\ell, \ell'}$, eq. (27).
7. Bin the coupling matrices to obtain M_{ℓ_b, ℓ'_b} , eq. (41).
8. Compute the pseudo-inverse of M_{ℓ_b, ℓ'_b} and obtain $\hat{C}_{\ell'_b} = M_{\ell'_b, \ell_b}^{-1} \hat{D}_{\ell_b}$.

For E/B mode separation, use eq. (78) and (79) as discussed in section 4.2.1. Use iterative method if needed.

Output: Binned power spectra $\hat{C}_{\ell'_b}$ and the effective ℓ values for the bin ℓ'_b .

Algorithm 2 *i*MASTER for correlation functions

Input: Measured correlation functions $\hat{\xi}(\theta_b)$; Window correlation functions, $\hat{\xi}_W(\theta)$ and $\hat{\xi}_W(\theta_b)$; Model power spectra C_ℓ ; Binning operators B_θ , B_C (B_D if required); $w(\theta)$ defining the scale cuts.

Output: Binned power spectra \hat{C}_{ℓ_b} .

1. Compute the Hankel transform operator and its inverse.
 2. Compute the binned theory $\xi(\theta_b)$ using eq. (59) and obtain B_θ^{-1} .
 3. Bin the inverse Hankel transform operator, eq. (67).
 4. Obtain pseudo- C_ℓ power spectra, eq. (69).
- For cosmic shear E/B power spectra, use eq. (76) and (77).
5. Obtain W_ℓ using inverse Hankel transform of $w(\theta)$.
 6. Go to step 3. of the algorithm 1: *i*MASTER for power spectra.

modeling as well as the issues relevant to imposing scale cuts.

In section 2, we derived the expressions for the over density field and the expressions for shot noise contributions to the two different estimators. We showed that the window effectively acts as the inverse noise weight and hence window weighted estimator has in general lower noise compared to the estimator in which the window is removed. In the noise dominated regime, this estimator is nearly equivalent to the quadratic estimator (FKP) for the gaussian field and thus for many LSS surveys, which are still noise dominated on most scales, is close to optimal. While the focus of discussion was using maps, in sections 2 and 4.1, we also discussed that applying systematics weights on galaxies, as is commonly done, is equivalent of the suboptimal estimator and it is better to apply such weights on the randoms. It is also worth remembering that the arguments we presented are equally valid along the line of sight (redshift) direction and in fact most of the studies in the literature apply the window weighting along the redshift direction. The $\frac{dn}{dz}$ weights that enter the C_ℓ model calculations are the redshift window weights and in the spectroscopic analysis BOSS collaboration (e.g. Ross et al. 2020; Alam et al. 2016) applied the FKP weights along the redshift space.

We also discussed the impact of the window estimation on the various estimators. In terms of the over density field, both estimators we discussed in section 2 are affected similarly by the biases in window estimation and using the sub-optimal estimator does not in any way help with the problem of window modeling (even in the absence of biases, one still need to model the mask which is not much easier). In section 3.4 we studied the impact of these window biases on the estimation of the pseudo- C_ℓ power spectra. Window biases lead to both additive and multiplicative biases in the power spectra. Additive biases have received some attention in the literature (e.g. Ross et al. 2012; Leistedt et al. 2013). Multiplicative biases while higher order, can be equally concerning for measurements with O(1%) precision requirements. We also saw that these biases can be more important at smaller scales (high ℓ) which contribute a large fraction of the cosmological information.

It is also worth stressing that these issues are equally applicable to tracers such as galaxy shear. In the case of shear, we normally think of multiplicative and additive biases on the ensemble bases. However, if these biases vary with the photometric conditions of the survey, then they can also be thought of as the part of the window and can be modeled using the methods in this paper and elsewhere in the literature.

In section 3 we studied the estimator for the measurement of the power spectra, namely the pseudo- C_ℓ estimator and the algorithms used in the modeling. We discussed the pesky issues involved in estimating the coupling matrices which can get quite complex for a non trivial window or for a power spectra that falls slowly or is nearly flat. For such cases the window needs to be estimated accurately out to very high ℓ , consistent with our discussion on systematics. In terms of algorithms, we saw that the standard MASTER algorithm can be biased due to incorrect assumptions about the scaling of the power spectra and our improved *i*MASTER algorithm corrects for those biases by using the correct power spectra from the model. This algorithm is more powerful than the existing algorithms (e.g. Alonso et al. 2019) as it allows direct comparison with unbinned theoretical models computed at effective bin centers, ℓ_b (i.e. binning is performed analytically) and does not require any corrections to be applied. Furthermore, the algorithm is also more optimal as it allows for cleaner extraction of information for a given set of scales by undoing the effects of mode mixing in the pseudo- C_ℓ estimator. We list the steps involved in *i*MASTER computation in the algorithm 1.

In section 4, we generalized the *i*MASTER algorithm to the correlation functions. Using this algorithm it is possible to reconstruct the power spectra from the correlation functions, including the E/B mode separation, though it can be hard (coupling matrix is complex) if the range of scales at which correlation function is measured is limited. Similar to the case of pseudo- C_ℓ mentioned earlier, power spectra modes reconstructed from correlation functions via *i*MASTER can be directly compared with unbinned theoretical models computed at effective bin centers (i.e. binning+window corrections are performed within the algorithm) and do not require any corrections to be applied. Steps involved in reconstruction of power spectra from correlation functions are listed in the algorithm 2. We also developed the proper method to convolve the correlation func-

tions in order to account for the scale cuts on the model in the Fourier space. This method prevents the leakage of information from the scales in Fourier space that are not properly modeled.

The iMASTER algorithm is also useful in speeding up the computations (during sampling) as after the initial setup, the computational complexity is reduced to $O(N_{\text{bin}}^2)$ instead of $O(\ell_{\text{max}}^2)$. That being said, the performance of these algorithms becomes even more important in the memory management during a large analysis, such as an LSST like 3×2 analysis, where the amount of peak memory requirement for the analysis decreases from $O(N_{\text{corr}} \times \ell_{\text{max}}^2)$ to $O(N_{\text{corr}} \times N_{\text{bin}}^2)$, where $N_{\text{corr}} \sim O(100)$ is the number of correlation pairs. For these large analysis, it will become imperative to use such an algorithm for computationally fast and efficient sampling of the large parameter spaces.

AVAILABILITY OF DATA & CODE

No new data were generated or analyzed in support of this research.

The code used for the computations in this paper is available at https://github.com/sukhdeep2/Skylens_public/tree/imaster_paper/.

ACKNOWLEDGEMENTS

I would like to thank Yin Li for many stimulating discussions that have helped me in this work and for providing detailed feedback on this manuscript. I also thank James Sullivan, Tanveer Karim and Mehdi Rezaie for helpful discussions and feedback on this work. I also thank the anonymous referee for several helpful comments and questions that helped in improving the presentation and explanations in the paper.

I am supported by the McWilliams fellowship at the Carnegie Mellon university. Part of this work was done at University of California, Berkeley, where I was supported by a postdoctoral fellowship at the Berkeley center for cosmological physics.

REFERENCES

- Abazajian K. N., et al., 2016, arXiv e-prints, p. [arXiv:1610.02743](#)
 Abbott T. M. C., et al., 2020, *Phys.Rev.D*, **102**, 023509
 Ade P., et al., 2019, *J. Cosmology Astropart. Phys.*, **2019**, 056
 Alam S., et al., 2016, preprint, ([arXiv:1607.03155](#))
 Alonso D., Sanchez J., Slosar A., LSST Dark Energy Science Collaboration 2019, *MNRAS*, **484**, 4127
 Baddour N., 2014, *SpringerPlus*, **3**, 246
 Baldauf T., Smith R. E., Seljak U., Mandelbaum R., 2010, *Phys.Rev.D*, **81**, 063531
 Bohm G., Zech G., 2014, *Nuclear Instruments and Methods in Physics Research A*, **748**, 1
 Bridle S. L., Crittenden R., Melchiorri A., Hobson M. P., Kneissl R., Lasenby A. N., 2002, *MNRAS*, **335**, 1193
 DES Collaboration et al., 2017, preprint, ([arXiv:1708.01530](#))
 Di Valentino E., et al., 2020, arXiv e-prints, p. [arXiv:2008.11284](#)
 Doré O., et al., 2014, arXiv e-prints, p. [arXiv:1412.4872](#)
 Dore O., et al., 2019, *BAAS*, **51**, 341
 Doux C., et al., 2021, *MNRAS*,
 Efstathiou G., 2004, *MNRAS*, **349**, 603
 Elsner F., Leistedt B., Peiris H. V., 2017, *MNRAS*, **465**, 1847
 Elvin-Poole J., et al., 2018, *Phys.Rev.D*, **98**, 042006
 Everett S., et al., 2020, arXiv e-prints, p. [arXiv:2012.12825](#)
 Feldman H. A., Kaiser N., Peacock J. A., 1994, *ApJ*, **426**, 23
 Górski K. M., Hivon E., Banday A. J., Wandelt B. D., Hansen F. K., Reinecke M., Bartelmann M., 2005, *ApJ*, **622**, 759
 Hamana T., et al., 2020, *PASJ*, **72**, 16
 Hamilton A. J. S., 1997, *MNRAS*, **289**, 285
 Heymans C., et al., 2021, *A&A*, **646**, A140
 Hivon E., Górski K. M., Netterfield C. B., Crill B. P., Prunet S., Hansen F., 2002, *ApJ*, **567**, 2
 Joachimi B., et al., 2021, *A&A*, **646**, A129
 LSST Dark Energy Science Collaboration 2012, arXiv e-prints, p. [arXiv:1211.0310](#)
 Landy S. D., Szalay A. S., 1993, *ApJ*, **412**, 64
 Lange J. U., Leauthaud A., Singh S., Guo H., Zhou R., Smith T. L., Cyr-Racine F.-Y., 2021, *MNRAS*, **502**, 2074
 Leistedt B., Peiris H. V., Mortlock D. J., Benoit-Lévy A., Pontzen A., 2013, *MNRAS*, **435**, 1857
 Levi M., et al., 2019, in Bulletin of the American Astronomical Society. p. 57 ([arXiv:1907.10688](#))
 Li Y., Singh S., Yu B., Feng Y., Seljak U., 2019, *J. Cosmology Astropart. Phys.*, **2019**, 016
 Neveux R., et al., 2020, *MNRAS*, **499**, 210
 Ng K.-W., Liu G.-C., 1999, *International Journal of Modern Physics D*, **8**, 61
 Planck Collaboration et al., 2020, *A&A*, **641**, A8
 Rezaie M., Seo H.-J., Ross A. J., Bunescu R. C., 2020, *MNRAS*, **495**, 1613
 Ross A. J., et al., 2012, *MNRAS*, **424**, 564
 Ross A. J., et al., 2020, *MNRAS*, **498**, 2354
 Schaan E., White M., 2021, arXiv e-prints, p. [arXiv:2103.01971](#)
 Schneider P., Eifler T., Krause E., 2010, *A&A*, **520**, A116
 Singh S., Mandelbaum R., Seljak U., Slosar A., Vazquez Gonzalez J., 2017, *MNRAS*, **471**, 3827
 Singh S., Mandelbaum R., Seljak U., Rodríguez-Torres S., Slosar A., 2020, *MNRAS*, **491**, 51
 Slosar A., Seljak U., Makarov A., 2004, *Phys. Rev. D*, **69**, 123003
 Wandelt B. D., Hivon E., Górski K. M., 2001, *Phys.Rev.D*, **64**, 083003
 Weinberg D. H., Mortonson M. J., Eisenstein D. J., Hirata C., Riess A. G., Rozo E., 2013, *Phys.Rep.*, **530**, 87

APPENDIX A: COMPARISON OF WINDOW WEIGHTING ON NOISE

In this appendix we prove the claim from section 2.1 that $\left[\overline{\frac{1}{W(\mathbf{x})}}\right] \geq \bar{W}(\mathbf{x})$.

We begin by noting that by $W(\mathbf{x}) \in [0, \infty)$ and $\bar{W}(\mathbf{x}) = 1$. For the case $W(\mathbf{x}) \in [0, \infty)$, proof is trivial as $\left[\overline{\frac{1}{W(\mathbf{x})}}\right] \rightarrow \infty$. Hence we will focus on the case $W(\mathbf{x}) \in (0, \infty)$ (i.e. 0 is excluded).

We can write $W(\mathbf{x})$ in terms of a mean zero variable as

$$W(\mathbf{x}) = 1 + w(\mathbf{x}), \quad (\text{A1})$$

where

$$\bar{W}(\mathbf{x}) = 1 + \bar{w}(\mathbf{x}) = 1, \quad \bar{w}(\mathbf{x}) = 0. \quad (\text{A2})$$

The mean of $1/W(\mathbf{x})$ is then

$$\left[\overline{\frac{1}{W_g(\mathbf{x})}}\right] = \left[\overline{\frac{1}{1 + w(\mathbf{x})}}\right]. \quad (\text{A3})$$

Defining $y = w(\mathbf{x})$ and rewriting we get

$$\left[\overline{\frac{1}{W_g(\mathbf{x})}}\right] = \int_{-1}^{\infty} \frac{1}{1+y} P(y) dy = \int_{-1}^1 \frac{1}{1+y} P(y) dy + \int_1^{\infty} \frac{1}{1+y} P(y) dy. \quad (\text{A4})$$

$P(y)$ is the probability distribution and in the second step we split the integral into two ranges, $y \in (-1, 1)$ and $y \in [1, \infty)$. Using the Taylor series in the first integral, we get

$$\left[\overline{\frac{1}{W_g(\mathbf{x})}}\right] = \int_{-1}^1 \left[1 + \sum_i (-1)^i y^i\right] P(y) dy + \int_1^{\infty} \frac{1}{1+y} P(y) dy \quad (\text{A5})$$

$$= \int_{-1}^1 dy P(y) (1 - y) + \int_{-1}^1 dy P(y) ([y^2 - y^3] + [y^4 - y^5] \dots) + \int_1^{\infty} \frac{1}{1+y} P(y) dy. \quad (\text{A6})$$

$$(\text{A7})$$

Now we use the fact that $\langle y \rangle = 0$ and $\int_{-1}^{\infty} P(y) = 1$, to change the limits of the first integral from $y \in (-1, 1)$ to $y \in [1, \infty)$

$$\left[\overline{\frac{1}{W_g(\mathbf{x})}}\right] = 1 + \int_1^{\infty} dy P(y) (-1 + y) + \int_{-1}^1 dy P(y) ([y^2 - y^3] + [y^4 - y^5] \dots) + \int_1^{\infty} \frac{1}{1+y} P(y) dy \quad (\text{A8})$$

$$= 1 + \int_{-1}^1 dy P(y) ([y^2 - y^3] + [y^4 - y^5] \dots) + \int_1^{\infty} \frac{y^2}{1+y} P(y) dy \geq 1. \quad (\text{A9})$$

Notice that the quantities inside square brackets, [], are always positive and the last integral is also non negative, thus proving that $\left[\overline{\frac{1}{W_g(\mathbf{x})}}\right] \geq 1$

APPENDIX B: MORE GENERAL WEIGHTING

In this appendix we derive the window and the noise effects in estimator of eq. (3) when more general weighting schemes are used.

Typically in a LSS survey, the galaxies are assigned weights which may depend on some intrinsic property of galaxy, we call such weights $w_{0,i}$ and another weight dependent on the variance, $w_{v,i}$, such that the total weight is given by

$$w_i = w_{0,i} w_{v,i} \quad (\text{B1})$$

The inverse variance weight is usually written as

$$w_{v,i} = \frac{N}{\text{Var}_i} = \frac{N}{C + \sigma_{m,i}^2}, \quad (\text{B2})$$

where $\sigma_{m,i}^2$ is contributed by the measurement noise and C is the sampling noise in galaxy field. $C = 1$ for galaxies and $C = \sigma_e^2$, i.e. shape noise, for shear. N is the normalization of the weights. The observed effective number of galaxies in a pixel are then

$$n_g(\mathbf{x}) = \sum_i w_i = \langle n_g(\mathbf{x}) \rangle \bar{w}_i(\mathbf{x}) (1 + \delta(\mathbf{x})). \quad (\text{B3})$$

$\bar{w}_i(\mathbf{x})$ is mean of weights within the pixel. The windowed overdensity field is

$$\delta_{g,W}(\mathbf{x}) = \frac{n_g(\mathbf{x})}{\bar{n}_g \bar{w}_i} - \frac{\langle n_g(\mathbf{x}) \rangle}{\bar{n}_g \bar{w}_i}. \quad (\text{B4})$$

\bar{w}_i is the sample mean of all the weights and is usually normalized to be 1. The window in this case is,

$$W_g(\mathbf{x}) = \frac{\langle n_g(\mathbf{x}) \rangle \bar{w}_i(\mathbf{x})}{\bar{n}_g \bar{w}_i}. \quad (\text{B5})$$

The variance is given as

$$\delta_N^2(\mathbf{x}) = \frac{1}{\bar{n}_g^2 \bar{w}_i^2} \sum_i w_i^2 \text{Var}_i = \frac{N}{\bar{n}_g^2 \bar{w}_i^2} \sum_i w_{0,i}^2 w_{v,i}. \quad (\text{B6})$$

Assuming that $w_{0,i}$ and $w_{v,i}$ are uncorrelated, we can write the sum as

$$\sum_i w_{0,i}^2 w_{v,i} = \langle n_g(\mathbf{x}) \rangle w_{v,i}(\mathbf{x}) w_{0,i}^2(\mathbf{x}), \quad (\text{B7})$$

to obtain

$$\langle \delta_N^2(\mathbf{x}) \rangle = N \frac{\langle n_g(\mathbf{x}) \rangle w_{v,i}(\mathbf{x}) w_{0,i}^2(\mathbf{x})}{\bar{n}_g^2 \bar{w}_i^2} = N \frac{W_g(\mathbf{x}) w_{0,i}^2(\mathbf{x})}{\bar{n}_g \bar{w}_i w_{0,i}(\mathbf{x})}. \quad (\text{B8})$$

Averaging over the survey we get

$$\langle \delta_N^2 \rangle = N \frac{\bar{W}_g}{\bar{n}_g \bar{w}_{v,i}} \frac{\bar{w}_{0,i}^2}{\bar{w}_{0,i} \bar{w}_{0,i}}. \quad (\text{B9})$$

Sometimes shot noise is described in terms of effective number density of galaxies, where

$$\frac{1}{n_g^{eff}} = \frac{1}{\bar{n}_g} \frac{\bar{w}_{0,i}^2}{\bar{w}_{0,i} \bar{w}_{0,i}}. \quad (\text{B10})$$

Notice that in the absence of $w_{0,i}$ eq. (B9) is equivalent to eq. (15) (in eq. (15) $N = 1$).

In general the additional weights do change the window as well as the dependence of noise in the window. Since we only worked with shot noise in this paper and subtracted out the correct noise from pseudo- C_ℓ measurements, this does not affect the results in the main part of this paper. However, these results highlight the dependence of noise on the window and weighting and such dependencies will need to be carefully modeled both for noise modeling and covariance matrix calculations.

APPENDIX C: WINDOW COUPLING MATRIX

In this appendix we derive the response of the pseudo- C_ℓ power spectra to window power spectra.

From Hivon et al. (2002), the pseudo- C_ℓ power spectra is given as

$$D_\ell = \sum_{\ell'} C_{\ell'} \frac{(2\ell' + 1)}{4\pi} \sum_{\ell''} W_{\ell''} (2\ell'' + 1) \begin{pmatrix} \ell & \ell' & \ell'' \\ s_1 & -s_1 & 0 \end{pmatrix} \begin{pmatrix} \ell & \ell' & \ell'' \\ s_2 & -s_2 & 0 \end{pmatrix}, \quad (\text{C1})$$

$$D_\ell = M_{\ell,\ell'} C_{\ell'}, \quad (\text{C2})$$

where in second equation we used the definition of the coupling matrix from eq. (27).

In eq. (C3), we can switch the order of summation over ℓ' and ℓ'' to write

$$D_\ell = \sum_{\ell''} W_{\ell''} \frac{(2\ell'' + 1)}{4\pi} \sum_{\ell'} C_{\ell'} (2\ell' + 1) \begin{pmatrix} \ell & \ell' & \ell'' \\ s_1 & -s_1 & 0 \end{pmatrix} \begin{pmatrix} \ell & \ell' & \ell'' \\ s_2 & -s_2 & 0 \end{pmatrix}, \quad (\text{C3})$$

$$D_\ell = M_{\ell,\ell''}^W W_{\ell''}, \quad (\text{C4})$$

where

$$M_{\ell,\ell''}^W = \frac{(2\ell'' + 1)}{4\pi} \sum_{\ell'} C_{\ell'} (2\ell' + 1) \begin{pmatrix} \ell & \ell' & \ell'' \\ s_1 & -s_1 & 0 \end{pmatrix} \begin{pmatrix} \ell & \ell' & \ell'' \\ s_2 & -s_2 & 0 \end{pmatrix}. \quad (\text{C5})$$

We can also use the symmetries of wigner-3j symbols to change the ordering of ℓ', ℓ'' if desired.

From eq. (C3) and (C4), we notice that the pseudo- C_ℓ power spectra is symmetric in its response to the window and the underlying density field we wish to study. This highlights the importance of modeling window properly and we used the eq. (C4) to study the impact the multiplicative biases in window (biased $W_{\ell''}$) have on D_ℓ .

APPENDIX D: CORRELATION FUNCTIONS

Here we derive the expressions for correlation functions in the presence of a survey window. We closely follow the expressions in Ng & Liu (1999).

We begin by writing the two point correlation function in presence of windows as

$$\langle \delta_1 \delta_2 \rangle(\theta) = \frac{1}{\xi_W(\theta)} \int d^2 \theta' \delta_1(\theta') \delta_2(\theta' + \theta) W_1(\theta') W_2(\theta' + \theta) \quad (D1)$$

$$= \frac{1}{\xi_W(\theta)} \int d^2 \theta' \sum_{l_1-4, m_1-4} \delta_{l_1, l_1, m_1} \delta_{l_2, l_2, m_2} W_1(l_3, m_3) W_2(l_4, m_4) {}_{s_1} Y_{\ell_1, m_1}(\theta') {}_{s_2} Y_{\ell_2, m_2}(\theta' + \theta) Y_{l_3, m_3}(\theta') Y_{l_4, m_4}(\theta' + \theta), \quad (D2)$$

where in the second equation we simply wrote the δ_i and W_i in terms of their spherical harmonic transforms (equivalent of Fourier Transform on a sphere).

Noting that $\delta_{l_1, l_1, m_1} \delta_{l_2, l_2, m_2} = C_{\ell_1} \delta_D(l_1, l_2) \delta_D(m_1, m_2)$, we get

$$\langle \delta_1 \delta_2 \rangle(\theta) = \frac{1}{\xi_W(\theta)} \int d^2 \theta' \sum_{l_1-4, m_1-4} C_{\ell_1} \delta_D(l_1, l_2) \delta_D(m_1, m_2) W_1(l_3, m_3) W_2(l_4, m_4) {}_{s_1} Y_{\ell_1, m_1}(\theta') {}_{s_2} Y_{\ell_2, m_2}(\theta' + \theta) Y_{l_3, m_3}(\theta') Y_{l_4, m_4}(\theta' + \theta), \quad (D3)$$

$$\langle \delta_1 \delta_2 \rangle(\theta) = \frac{1}{\xi_W(\theta)} \int d^2 \theta' \sum_{l_1, 3, 4, m_1, 3, 4} C_{\ell_1} W_1(l_3, m_3) W_2(l_4, m_4) {}_{s_1} Y_{\ell_1, m_1}(\theta') {}_{s_2} Y_{\ell_1, m_1}(\theta' + \theta) Y_{l_3, m_3}(\theta') Y_{l_4, m_4}(\theta' + \theta). \quad (D4)$$

Where in the second step I carried out the sums over δ_D . Now we use the spherical harmonics identity (Ng & Liu 1999), $\sum_m {}_{s_1} Y_{\ell_1, m_1}(\theta') {}_{s_2} Y_{\ell_1, m_1}(\theta' + \theta) = \sqrt{\frac{2\ell_1+1}{4\pi}} (-1)^{s_1-s_2} {}_{s_1} Y_{\ell_1, s_2}(\theta)$ to obtain

$$\langle \delta_1 \delta_2 \rangle(\theta) = \frac{1}{\xi_W(\theta)} \int d^2 \theta' \sum_{l_1, 3, 4, m_1, 3, 4} C_{\ell_1} W_1(l_3, m_3) W_2(l_4, m_4) {}_{-s_1} Y_{\ell_1, s_2}(\theta) Y_{l_3, m_3}(\theta') Y_{l_4, m_4}(\theta' + \theta), \quad (D5)$$

where I omitted the $(-1)^{s_1-s_2}$ factor since s_1 and s_2 are even numbers for the tracers we use. Rearranging the terms, we get

$$\langle \delta_1 \delta_2 \rangle(\theta) = \frac{1}{\xi_W(\theta)} \sum_{\ell_1} \sqrt{\frac{2\ell_1+1}{4\pi}} {}_{-s_1} Y_{\ell_1, s_2}(\theta) C_{\ell_1} \int d^2 \theta' \sum_{l_3, 4, m_3, 4} W_1(l_3, m_3) W_2(l_4, m_4) Y_{l_3, m_3}(\theta') Y_{l_4, m_4}(\theta' + \theta). \quad (D6)$$

$$= \frac{1}{\xi_W(\theta)} \sum_{\ell_1} \sqrt{\frac{2\ell_1+1}{4\pi}} {}_{-s_1} Y_{\ell_1, s_2}(\theta) C_{\ell_1} \xi_W(\theta). \quad (D7)$$

The term inside the integral is simply the correlation function of the window, denoted by $\xi_W(\theta)$.

Using

$${}_{-s_1} Y_{\ell_1, s_2}(\theta, \phi) = \sqrt{\frac{2\ell_1+1}{4\pi}} {}_{-s_1} d_{\ell_1, s_2}(\cos(\theta)) e^{-is\phi}, \quad (D8)$$

and carrying out the angular integrals (see discussion in Ng & Liu 1999), we obtain

$$\langle \delta_1 \delta_2 \rangle(\theta) = \frac{\xi_W(\theta)}{\xi_W(\theta)} \sum_{\ell_1} \frac{2\ell_1+1}{4\pi} {}_{s_1} d_{\ell_1, s_2}(\cos \theta) C_{\ell_1}. \quad (D9)$$

We used the full sky averaging expressions from eq. 7.3 of Ng & Liu (1999), to simplify the window correlation function, i.e.

$$\xi_W(\theta) = \sum_{\ell_1} \sqrt{\frac{2\ell_1+1}{4\pi}} {}_0 Y_{\ell, 0}(\theta) W_{\ell} = \sum_{\ell_1} \frac{2\ell_1+1}{4\pi} {}_0 d_{\ell, 0}(\cos(\theta)) W_{\ell} = \xi_W(\theta). \quad (D10)$$

W_{ℓ} is the pseudo- C_{ℓ} power spectra of the window.

While the window effect appears to cancel in eq. (D9), as discussed in section 4.1, the binning operator act separately on numerator and denominator, hence the window effects do not fully cancel. Therefore the correlation functions are still sensitive to the window and here we have shown that the window effects separate out from the density field such that the estimator is only sensitive to the correlation function of the window.

APPENDIX E: SCALE CUTS

E1 D_{ℓ} reconstruction from ξ

Here we show that the inverse Hankel transform of correlation functions measured over limited range of scales leads to pseudo- C_{ℓ} power spectra. This proof also shows the equivalence of correlation function and pseudo- C_{ℓ} power spectra when window correlation function $\xi_W(\theta)$ is used in place of $w(\theta)$ in the equations below.

For scale cuts on correlation functions, we have

$$D_{\ell} = 2\pi \int d\theta \sin(\theta) \xi(\theta) w(\theta) \sqrt{\frac{4\pi}{2\ell+1}} {}_{-s_1} Y_{\ell, s_2}(\theta). \quad (E1)$$

Writing $\xi(\theta)$ and $w(\theta)$ in terms of their Fourier counterparts, we get

$$D_\ell = \sum_{\ell_1, \ell_2} C_{\ell_1} w_{\ell_2} \sqrt{\frac{2\ell_1 + 1}{4\pi}} \sqrt{\frac{2\ell_2 + 1}{4\pi}} \int d\theta \sin(\theta)_{-s_1} Y_{\ell, s_2}(\theta)_{-s_1} Y_{\ell_1, s_2}(\theta)_{-s_{1w}} Y_{\ell_2, s_{2w}}(\theta), \quad (\text{E2})$$

$$D_\ell = \sum_{\ell_1, \ell_2} C_{\ell_1} w_{\ell_2} \sqrt{\frac{4\pi}{2\ell + 1}} \frac{(2\ell_1 + 1)(2\ell_2 + 1)}{4\pi} \sqrt{\frac{2\ell + 1}{4\pi}} \begin{pmatrix} \ell & \ell_1 & \ell_2 \\ s_2 & -s_2 & s_{2w} \end{pmatrix} \begin{pmatrix} \ell & \ell_1 & \ell_2 \\ s_1 & -s_1 & s_{1w} \end{pmatrix}, \quad (\text{E3})$$

$$D_\ell = \sum_{\ell_1, \ell_2} C_{\ell_1} w_{\ell_2} \frac{(2\ell_1 + 1)(2\ell_2 + 1)}{4\pi} \begin{pmatrix} \ell & \ell_1 & \ell_2 \\ s_2 & -s_2 & s_{2w} \end{pmatrix} \begin{pmatrix} \ell & \ell_1 & \ell_2 \\ s_1 & -s_1 & s_{1w} \end{pmatrix}, \quad (\text{E4})$$

where in the second equation we wrote the integral over three spherical harmonics in terms of the wigner-3j function and the last equation is very similar to eq. (C3), with $s_{1w} = s_{2w} = 0$. As stated earlier, we can replace $w(\theta)$ with the correlation function of the window $\xi_W(\theta)$ in which case $w(\ell_2)$ gets replaced with the window power spectra $W(\ell_2)$ and we obtain the expressions identical to eq. (C3), thus showing that the power spectra and correlation function estimators are identical when full range of scales in ℓ, θ is used.

E2 Modeling ξ with cuts on C_ℓ

Here we derive the expressions for convolution operator acting on the correlation functions to account for the model cuts in the Fourier space.

We wish to derive the method to correct ξ for model cuts in the ℓ space, i.e.

$$\xi_{cut}(\theta) = \sum_{\ell} b_{\ell} C_{\ell} \sqrt{\frac{2\ell + 1}{4\pi}} s_1 Y_{\ell, s_2}(\theta). \quad (\text{E5})$$

b_{ℓ} is the function that applies the cuts in ℓ .

Following Baddour (2014), we make an ansatz that

$$\xi_{cut}(\theta) = \int_0^{2\pi} d\phi_1 \int d\theta_1 \sin(\theta_1) \xi(\theta_1) b(\theta, \theta_1), \quad (\text{E6})$$

where

$$b(\theta, \theta_1) = \sum_{\ell} b_{\ell} \frac{2\ell + 1}{4\pi} s_1 Y_{\ell, s_2}(\theta)_{s_1} Y_{\ell, s_2}(\theta_1). \quad (\text{E7})$$

Plugging $b(\theta, \theta_1)$ back we get

$$\xi_{cut}(\theta) = \int d\phi_1 \int d\theta_1 \sin(\theta_1) \sum_{\ell} b_{\ell} \frac{2\ell + 1}{4\pi} s_1 Y_{\ell, s_2}(\theta)_{s_1} Y_{\ell, s_2}(\theta_1) \sum_{\ell_1} C_{\ell_1} \sqrt{\frac{2\ell + 1}{4\pi}} s_1 Y_{\ell_1, s_2}(\theta_1)_{s_1}, \quad (\text{E8})$$

$$= \sum_{\ell} b_{\ell} C_{\ell} \sqrt{\frac{2\ell + 1}{4\pi}} s_1 Y_{\ell, s_2}(\theta). \quad (\text{E9})$$

Hence showing that eq. (E6) is equivalent to eq. (E5).

APPENDIX F: SIMULATIONS

This appendix describes the simulations and the assumptions about data samples used in the examples presented in the paper.

For shear, we used a LSST shear sample properties, with $\bar{n}_g = 26 \text{ arcminutes}^{-2}$, $f_{sky} = 0.3$, shape noise $\sigma_{\gamma} = 0.26$ per component. All the galaxies are assumed to be in a narrow redshift bin at $z = 1$. For the galaxy sample, we used $\bar{n}_g = 10 \text{ arcminutes}^{-2}$, $f_{sky} = 0.3$, $b_g = 1$. Magnification and intrinsic alignments are set to be zero.

Fig. F1 shows the two different window functions used in the examples presented in main part of the paper.

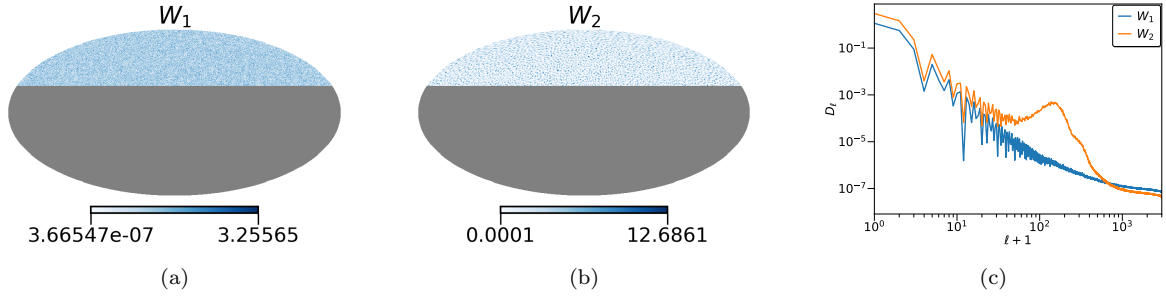


Figure F1. Window functions used for the simulations as well as other calculations using windows in the main part of the paper. W_1 is obtained using same C_ℓ as the galaxy sample ($C_{\ell,gg}$) and represents a realistic window for the case galaxy shear. W_2 represents a more complex window with an additional gaussian power spectra ($C_{\ell,gg} + C_{\ell,\text{gaussian}}$), where $C_{\ell,\text{gaussian}}$ peaks at $\ell \sim 200$ and has the width of $\sigma \sim 50$. Both windows have constants added such that the minimum value is 0. c) The power spectra of two windows.